

Figure 4. Transduction with C/EBP α -C^m alone induced AML in a mouse BMT model. (A) Kaplan-Meier analysis for the survival of mice that received transplants of BM cells transduced with C/EBP α -C^m-IG (C^m, n = 17), C/EBP α -N^m-IG (N^m, n = 8), or mock (pMYs-IG, n = 8). (B) Cytopsin preparations of BM cells derived from mice/C/EBP α -C^m (left) or mice/N^m (right) were stained with Giemsa. A representative photograph is shown. Images were obtained with a BX51 microscope and a DP12 camera (Olympus); objective lens, UplanFI (Olympus); original magnification $\times 100$. (C) Flow cytometric analysis of BM cells derived from mice/C/EBP α -C^m (middle), mice/C/EBP α -N^m (right), or mice/pMYs-IG (left). The dot plots show Ly5.1, Gr-1, CD11b, c-kit, B220, or CD19 labeled with phycoerythrin-conjugated monoclonal Ab versus expression of GFP. (D) Expression of C/EBP α -C^m protein and p30 protein generated by C/EBP α -N^m in spleen cells of mice/pMYs-IG (lane 1) and mice/C^m (lanes 2-4) (top) or in spleen cells of mice/pMYs-IG (lane 1) and mice/N^m (lanes 2-4) (bottom). Cell lysates were subject to immunoblotting with anti-C/EBP α (14AA) Ab or anti-tubulin Ab as control. Data are representative of 3 independent experiments. (E-F) Real-time PCR for G-CSF-R (E) or c-Myc (F) in BM cells derived from mice/C^m or mice/pMYs-IG. Expression levels were normalized by β -actin mRNA. The relative expression level of BM derived from mice/mock (lane 1) was defined as 1. All data points correspond to the mean and the standard deviation (SD) of 3 independent experiments. Lanes 1-2: mice/pMYs-IG; lanes 3-6: mice/C^m.

(3-5 months) compared with mice that had received transplants of BM cells expressing both Myc-C^m-IRES-GFP and mock (pMYs-IR, hereafter referred to as mice/Myc-C^m/pMYs-IR; Figure 5A). Of note, there was no significant difference of the phenotypes between mice/C^m and mice/Myc-C^m/pMYs-IR or between mice/N^m

and mice that had received transplants of BM cells expressing both mock (pMYs-IG) and Flag-N^m-IRES-dsRED (hereafter referred to as mice/pMYs-IG/Flag-N^m; Figures 4-5 and data not shown). The percentages of the immature blast ranged from 72%-94% in mice/Myc-C^m/Flag-N^m (Table 2) compared with 62%-92% in

Table 2. Characteristics of AML caused by C/EBP α mutants

	pMYs-IG/pMYs-IR (n = 8)	Myc-C ^m /pMYs-IR (n = 6)	Myc-C ^m /Flag-N ^m (n = 8)
WBC (/ μ L)	9060 \pm 1648	5816 \pm 3128	36 675 \pm 22 956
Hb (g/dL)	16.4 \pm 3.2	12.4 \pm 2.2	10.7 \pm 2.3
Plt ($\times 10^4$ / μ L)	79.4 \pm 43.1	7.2 \pm 4.5	19.8 \pm 13.1
BM count ($\times 10^7$)	3.34 \pm 0.73	1.69 \pm 0.30	2.83 \pm 0.88
Leukemic cells (%)	-	60-92	72-94
Liver weight (mg)	1433 \pm 153	2071 \pm 1281	2441 \pm 1315
Spleen weight (mg)	113 \pm 24	476 \pm 220	549 \pm 239

Averages and standard deviations are shown. BM cells were isolated from both tibiae and femurs.

WBC indicates white blood cell; Hb, hemoglobin; and Plt, platelets.

C/EBP α -C^m-induced leukemia (Table 2 and Figure 5B). Morphologies of the leukemic blasts are more immature in mice/Myc-C^m/Flag-N^m than mice/Myc-C^m/pMYs-IR (Figure 5B), consistent with the lower expression of Gr-1 in the former (Figure 5C and data not shown). Flow cytometric analysis delineated that most leukemic cells of mice/Myc-C^m/Flag-N^m expressed both GFP and dsRED (Figure 5C) and invariable markers: CD11b-inintermediate and Gr-1, B-220, c-kit-low (Figure 5C). Expression of both C/EBP α -C^m protein and p30 protein generated by C/EBP α -N^m in leukemic cells of mice/Myc-C^m/Flag-N^m was confirmed by Western blot analysis (Figure 5D). Expression levels of p30 protein generated by C/EBP α -N^m were not correlated with the disease latency in mice/Myc-C^m/Flag-N^m (Figure 5A,D). The morbid mice/Myc-C^m/Flag-N^m suffered from anemia and thrombocytopenia-like mice/Myc-C^m/pMYs-IR; however, it was of note that unlike mice/Myc-C^m/pMYs-IR, most mice/Myc-C^m/Flag-N^m exhibited marked leukocytosis (Figure 5E-F and Table 2). These results suggested that C/EBP α -N^m either confers a proliferative advantage on immature myeloid cells or collaborates with C/EBP α -C^m in blocking differentiation of myeloid cells in vivo. It is of note that this collaborative effect was induced by relatively low levels of p30 protein generated by C/EBP α -N^m.

C/EBP α -C^m, but not C/EBP α -N^m, collaborated with Flt3-ITD in inducing AML in a BMT model

Because C/EBP α -C^m possessed the potential to strongly suppress myeloid differentiation, this mutation could be categorized into class II mutations. We speculated that AML would be efficiently induced by combining C/EBP α -C^m with class I gene alterations. To test this, murine BM mononuclear cells, transduced with both Flt3-ITD and either C/EBP α -C^m or C/EBP α -N^m, were transplanted into the recipient mice. BM mononuclear cells expressing both mutants were recognized as GFP- and dsRED-double positive cells, 10%-20% of BM cells before the transplantation. As reported previously,⁴⁹ mice receiving transplants of BM cells expressing both Flt3-ITD-IRES-GFP and mock (pMYs-IR) (mice/FLT/pMYs-IR) developed myeloproliferative neoplasm (MPN) within 1.5-3 months after transplantation (Figure 6A). BM and spleen were occupied with increased numbers of mature myeloid cells expressing CD11b at high levels and Gr-1 at intermediate to high levels (Figure 6B-C). Intriguingly, mice transplanted with BM cells expressing both Flt3-ITD-IRES-GFP and C/EBP α -C^m-IRES-dsRED (mice/FLT/C^m) developed aggressive leukemia within 2-3 weeks after transplantation (Figure 6A). Histologic examination of mice/FLT/C^m showed that BM was occupied with the 2 populations: large and small blastlike cells (Figure 6B). However, flow cytometric analysis demonstrated that both populations, double positive for GFP and dsRED, similarly

expressed B220, CD19, Gr-1, and CD11b and could not be differentiated (Figure 6C and data not shown). Thus, mice/FLT/C^m invariably developed biphenotypic leukemia. Western blot analysis demonstrated that both Flt3-ITD and C/EBP α -C^m proteins were expressed in spleen cells of mice/FLT/C^m (Figure 6D). On the other hand, mice that received transplants of BM cells expressing both Flt3-ITD-IRES-GFP and C/EBP α -N^m-IRES-dsRED (mice/FLT/N^m) developed MPN with latencies comparable with those of MPN developed by mice/FLT/pMYs-IR, although some lymphoid blast cells were observed in 2 mice/FLT/N^m (Figure 6A and data not shown). Thus, C/EBP α -N^m did not significantly collaborate with Flt3-ITD in leukemogenesis in the present BMT model. Finally, leukemic cells derived from mice/FLT/C^m proliferated independently of IL-3 in the culture, while those from mice/C^m still required IL-3 for their growth. Leukemic cells derived from mice/FLT or mice/FLT/N^m did not survive even in the presence of IL-3. Moreover, we found stronger activation of STAT5, STAT3, AKT, and ERK in leukemic cell lines derived from mice/C^m/FLT compared with those from mice/C^m (Figure 6E). These results indicated that Flt3-ITD conferred additional proliferative potentials as a class I mutation on the cells expressing C/EBP α -C^m alone, thereby inducing aggressive leukemia.

Discussion

The present results on CEBPA mutations of AML patients confirmed previous reports²⁰⁻²⁸; CEBPA mutations are found in 5%-14% of de novo AML, and most of them harbor 2 distinct mutations on different alleles and have good prognosis. In addition, our results suggested that mutations of CEBPA are found only in one allele in most cases of therapy-related AML or MDS, and AML progressed from MDS harboring CEBPA mutations (8/71 and 7/224). While we did not find additional mutations in other genes in de novo AML patients with double CEBPA mutations, we detected 3 additional mutations in 15 patients with therapy-related AML or MDS and MDS/AML. These results indicate that a CEBPA mutation collaborates with either a different type of CEBPA mutations or mutations in different genes in inducing leukemia.

Analysis of CEBPA mutations in in vitro assays provided novel insights concerning the role of CEBP α in blood cells. C/EBP α -N^m and p30, but not C/EBP α -C^m, suppressed transcriptional activation of C/EBP α -WT in a luciferase assay using 293T cells (Figure 2A) as reported previously.²⁰ Curiously, expression of G-CSF-R, a major target of C/EBP α , was profoundly suppressed by C/EBP α -C^m but not by C/EBP α -N^m in 32Dcl3 cells (Figure 1F). C/EBP α -C^m suppressed G-CSF-induced granulocytic differentiation of 32Dcl3 cells more efficiently than C/EBP α -N^m (Figure 1D-E). It is possible that insufficient suppression of G-CSF-induced differentiation of 32Dcl3 cells by C/EBP α -N^m despite its inhibitory activity on transcriptional activation of C/EBP α -WT in 293T cells may be because of the low expression of C/EBP α -N^m in 32Dcl3 cells (Figure 1B). In fact, C/EBP α -p30 moderately suppressed the expression of G-CSF-R and inhibited G-CSF-induced differentiation of 32Dcl3 cells (Figure 1D-F). However, this does not explain why C/EBP α -C^m efficiently blocks the differentiation of 32Dcl3 cells despite its inability to suppress C/EBP α activation in the luciferase assay. Therefore, we speculated that C/EBP α mutants behave differently in epithelial 293T cells and hematopoietic 32Dcl3 cells and tested whether hematopoietic cell-specific transcription factors play some role in 32Dcl3 cells. Because it was

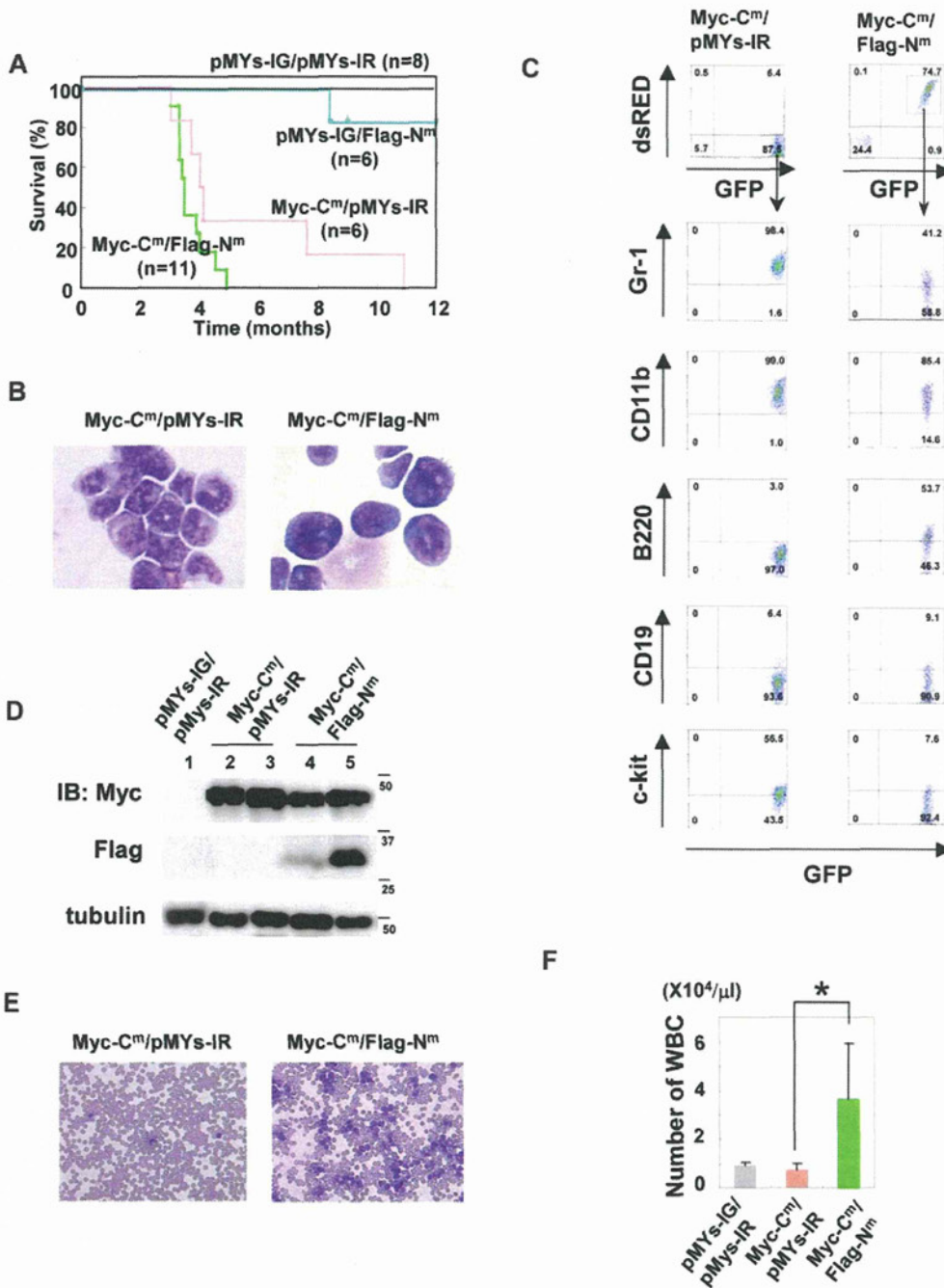


Figure 5. Coexpression of both C/EBP α -C^m and C/EBP α -N^m led to AML with leukocytosis with shorter latencies. (A) Kaplan-Meier analysis for the survival of mice that received transplants of BM cells transduced with both Myc-tagged C/EBP α -C^m-IG and pMYS-IR (Myc-C^m/pMYS-IR, n = 6), both pMYS-IG and Flag-tagged C/EBP α -N^m-IR (pMYS-IG/Flag-N^m, n = 6), both Myc-tagged C/EBP α -C^m-IG and Flag-tagged C/EBP α -N^m-IR (Myc-C^m/Flag-N^m, n = 11), or mock (pMYS-IG/pMYS-IR, n = 8). (B) Cytospin preparations of BM cells derived from mice/Myc-C^m/pMYS-IR or mice/Myc-C^m/Flag-N^m were stained with Giemsa. A representative photograph is shown. Images were obtained with a BX51 microscope and a DP12 camera (Olympus); objective lens, UplanFI (Olympus); original magnification $\times 100$. (C) Flow cytometric analysis of BM cells derived from mice/Myc-C^m/pMYS-IR (left) or mice/Myc-C^m/Flag-N^m (right). The dot plots show expression of dsRED versus expression of GFP (1st panel). In the indicated gating, the dot plots show expression of Gr-1, CD11b, B220, CD19, or c-kit labeled with phycoerythrin-Cy5-conjugated streptavidin versus expression of GFP. (D) Expression of Myc-tagged C/EBP α -C^m protein and p30 protein generated by Flag-tagged C/EBP α -N^m in BM cells derived from mice/pMYS-IG/pMYS-IR (lane 1), mice/Myc-C^m/pMYS-IR (lanes 2-3), or mice/Myc-C^m/Flag-N^m (lanes 4-5) was detected by using anti-Myc monoclonal Ab (top) and anti-Flag mAb (middle), respectively, in Western blot analysis. Equal loading was evaluated by probing the immunoblots with anti-tubulin Ab (bottom). Data are representative of 3 independent experiments. (E) Peripheral blood smears obtained from mice/Myc-C^m/pMYS-IR (left) or mice/Myc-C^m/Flag-N^m (right) were stained with Giemsa. Images were obtained with a BX51 microscope and a DP12 camera (Olympus); objective lens, UplanFI (Olympus); original magnification $\times 20$. (F) Counts of white blood cells (WBC) obtained from mice/Myc-C^m/pMYS-IR (n = 6), mice/Myc-C^m/Flag-N^m (n = 8), or mice/pMYS-IG/pMYS-IR (n = 8). All data points correspond to the mean and the standard deviation (SD). Statistically significant differences are shown. **P* < .05.

reported that PU.1 plays important roles in macrophage differentiation, which is hampered by its interaction with C/EBP α through its

C-terminal bZIP domain,⁵⁰ we investigated whether PU.1 plays some role in C/EBP α -C^m-mediated transcription. The present

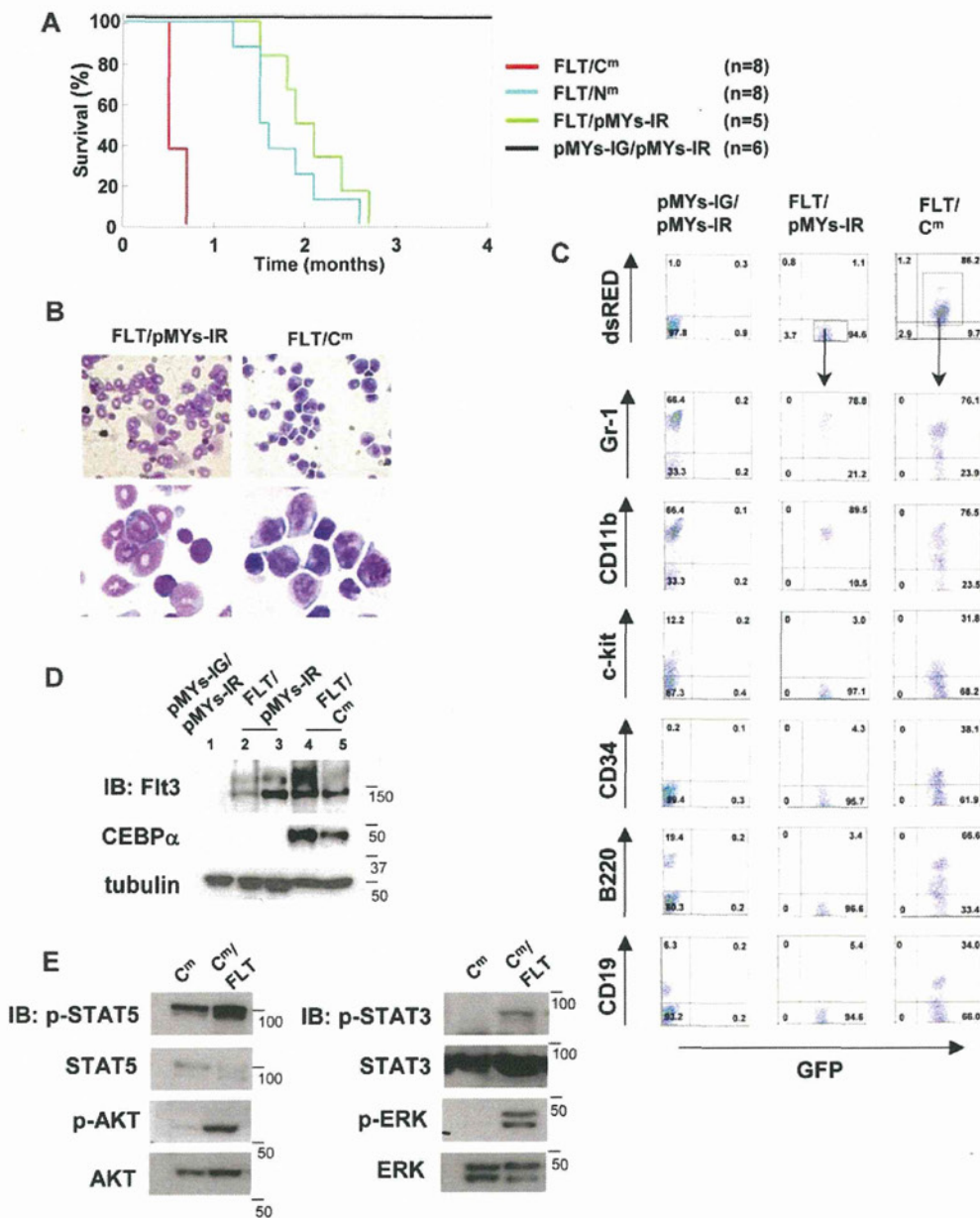


Figure 6. C/EBP α -C^m, but not C/EBP α -N^m, collaborated with FIt3-ITD in inducing aggressive AML. (A) Kaplan-Meier analysis for the survival of mice that received transplants of BM cells transduced with both FIt3-ITD-IG and pMYs-IR (FLT/pMYs-IR, n = 5), both FIt3-ITD-IG and C/EBP α -C^m-IR (FLT/C^m, n = 8), both FIt3-ITD-IG and C/EBP α -N^m-IR (FLT/N^m, n = 8), or mock (pMYs-IG/pMYs-IR, n = 8). (B) Cytopsin preparations of BM cells derived from mice/FLT/pMYs-IR or mice/FLT/C^m were stained with Giemsa. Images were obtained with a BX51 microscope and a DP12 camera (Olympus); objective lens, UplanFI (Olympus); original magnification $\times 40$ (top), $\times 100$ (bottom). (C) Flow cytometric analysis of BM cells derived from mice/pMYs-IG/pMYs-IR, mice/FLT/pMYs-IR, or mice/FLT/C^m. The dot plots show expression of dsRED versus expression of GFP (first panel). In the indicated gating, the dot plots show expression of Gr-1, CD11b, c-kit, CD34, B220, or CD19 labeled with phycoerythrin-Cy5-conjugated streptavidin versus expression of GFP. (D) Expression of C/EBP α -C^m or FIt3-ITD in spleen cells of mice/pMYs-IG/pMYs-IR (lane 1), mice/FLT/pMYs-IG (lanes 2-3), or mice/FLT/C^m (lanes 4-5) was detected by using anti-C/EBP α (14AA) Ab (middle) or anti-FIt3 Ab (top), respectively, in Western blot analysis. Equal loading was evaluated by probing the immunoblots with anti-tubulin Ab. Data are representative of 3 independent experiments. (E) Immortalized leukemic cells derived from mice/FLT/C^m had increased phosphorylation of STAT5, AKT, STAT3, and ERK compared with those from mice/C^m. Whole-cell extracts of the former cells (immortalized in the absence of IL-3) or the latter (immortalized in the presence of IL-3) were immunoblotted with phospho-specific Abs as described in the Methods. Equal loading was evaluated by reprobing the immunoblots with anti-STAT5, anti-AKT, anti-STAT3, or anti-ERK Abs. Data are representative of 3 independent experiments.

result indicated that C/EBP α synergized with exogenously expressed PU.1 in stimulating transcription of the target genes in 293T cells, which was profoundly inhibited by C/EBP α -C^m but not by C/EBP α -N^m (Figure 2B), and suggested that C/EBP α -C^m hampers PU.1 from interacting with other molecules including C/EBP α in hemopoietic cells, leading to inhibition of granulocytic differentiation.

As for cooperation between C/EBP α -N^m and C/EBP α -C^m in leukemogenesis, we demonstrated using BMT models that C/EBP α -N^m and C/EBP α -C^m in combination induced AML with shorter latencies compared with transplantation of C/EBP α -C^m-transduced BM cells alone. In addition, combining both mutations resulted in increased number of leukemic cells, implicating C/EBP α -N^m in expansion of the cells whose differentiation was

blocked by C/EBP α -C^m. Thus, these results suggested that C/EBP α -C^m works as a class II mutation while C/EBP α -N^m works as a class I mutation in inducing leukemia.³¹⁻³⁶ To test this hypothesis, we built another BMT model where BM cells transduced with Flt3-ITD and either C/EBP α -C^m or C/EBP α -N^m were transplanted to lethally irradiated mice. Flt3-ITD dramatically shortened the latency of leukemia induced by C/EBP α -C^m but not by C/EBP α -N^m, indicating that C/EBP α -C^m worked as a class II mutation in inducing leukemia. Transplantation of BM cells transduced with both C/EBP α -C^m and Flt3-ITD quickly induced leukemia in just 2 weeks after transplantation. Most of the transplanted mice seemed to develop biphenotypic leukemia as assessed on the morphology and surface marker expressions (Figure 6B-C). In our hands, BM cells transduced with Flt3-ITD sometimes induce lymphoid malignancies in addition to myeloproliferative disease,⁴⁹ bringing some complexity to the experiment. Nonetheless, dramatically shortened latencies with the combination of C/EBP α -C^m and Flt3-ITD strongly indicated that C/EBP α -C^m works as a class II mutation in inducing leukemia. On the other hand, because the expression levels of C/EBP α -N^m was low in our experiments, further experiments will be required to firmly demonstrate that C/EBP α -N^m plays a class I-like role. One possible experiment is to test a combination between C/EBP α -N^m and a known class II mutation. Nonetheless, a class I-like role of C/EBP α -N^m was suggested by the marked increase in the number of leukemic cells in mice/Myc-C^m/Flag-N^m compared with mice/Myc-C^m/pMYs-IR. In relation to this, although the "2-hit theory" well explain many clinical observations, additional classes of mutations may be required for the comprehensive understanding of leukemogenesis as proposed by Renneville et al⁵² In fact, we detected more than 3 mutations including mutations, chromosomal translocations, or deletions in 5 of 20 patients with leukemia and MDS (Table 1).

Concerning the in vivo effects of CEBPA mutations, several different results were reported.^{29,30,51-54} Bereshchenko et al³⁰ have recently published a report using knock-in mice that C/EBP α -p30 and a C-terminal mutation collaborated in inducing leukemia. Our results basically agreed with those by Bereshchenko et al. However, while our results implicated C-terminal mutations of C/EBP α in differentiation, leading to leukemia with relatively long latencies, Bereshchenko et al³⁰ suggested premalignant HSC expansion by C-terminal mutations. The reason for the disparity is not clear, but was partly caused by the difference in the strength or functions of different C-terminal mutants or in the expression levels of mutants in knock-in mice and BMT models. Concerning the experimental systems, knock-in mice are superior to mouse BMT models in several aspects as indicated previously.^{29,30} Most importantly, expression of the mutant C/EBP α is driven by the authentic promoter in knock-in mice while it is over-driven by an external promoter in BMT models. Moreover, replacement of both alleles with different C/EBP α mutations closely mimics human leukemia, as it lacks the WT C/EBP α unlike the BMT model. In

addition, in BMT models, retrovirus integration sites sometimes modify the phenotype of the disease. However, BMT models do have some advantages. First, in contrast to knock-in mice where all hemopoietic cells express the mutant allele, only some cells can be of a leukemia origin, which would more faithfully mimic human pathologic situations. In addition, various mutants can be readily tested in vivo. Bereshchenko et al³⁰ used K313dup as a C-terminal CEBPA mutation, demonstrating that mice^{K313dup/+} did not develop leukemia. K313dup was a weak inducer of leukemia in our BMT model, where only 1 of the 4 transplanted mice developed myeloid leukemia in 10 months (data not shown). On the other hand, C/EBP α -C^m, a C-terminal mutation with 304-323dup that we used in the present study, induced leukemia in most transplanted mice (Figure 4A). Thus, knock-in mice models and BMT models can complement with each other in investigating in vivo leukemogenesis.

To summarize, we have presented a series of evidence, including clinical data, in vitro experiments, and mouse BMT models, showing that 2 different mutations of CEBPA, C/EBP α -N^m and C/EBP α -C^m, play distinct roles in leukemogenesis. Moreover, our results strongly indicated that C/EBP α -C^m is able to play as a class II mutation in concert with Flt3-ITD in inducing leukemia. Further elucidation of the molecular mechanism of CEBPA mutations-induced leukemia may pave a novel way to treating patients with leukemia.

Acknowledgments

We thank Dr Atsushi Iwama, Dr Claus Nerlov, and Dr Shigekazu Nagata for kindly providing plasmids. We are grateful to Dr Dovie Wylie for her excellent editing of the English.

This work was supported by the Ministry of Education, Science, Technology, Sports and Culture, Japan and in part supported by Global COE Program "Center of Education and Research for the Advanced Genome-Based Medicine, for personalized medicine and the control of worldwide infectious diseases," MEXT, Japan.

Authorship

Contribution: N.K. did all the experiments and participated in writing the manuscript; J.K. oversaw all the experiments and actively participated in manuscript writing; N.D., Y.K., N.W.O., K.T., F.N., T.O., and Y.E. technically supported BMT; Y.F. and H.N. provided plasmids and reagents; Y.H. and H.H. provided and analyzed human samples; and T.K. conceived the project, secured funding, and actively participated in manuscript writing.

Conflict-of-interest disclosure: T.K. serves as a consultant for R&D Systems. The remaining authors declare no competing financial interests.

Correspondence: Toshio Kitamura, Division of Cellular Therapy and Division of Stem Cell Signaling, The Institute of Medical Science, The University of Tokyo, 4-6-1 Shirokanedai, Minato-ku, Tokyo 108-8639, Japan; e-mail: kitamura@ims.u-tokyo.ac.jp.

References

- Zhang P, Iwasaki-Arai J, Iwasaki H, et al. Enhancement of hematopoietic stem cell repopulating capacity and self-renewal in the absence of the transcription factor C/EBP alpha. *Immunity*. 2004;21(6):853-863.
- Tenen DG, Hromas R, Licht JD, Zhang D-E. Transcription factors, normal myeloid development, and leukemia. *Blood*. 1997;90(2):489-519.
- Friedman AD, McKnight SL. Identification of two polypeptide segments of CCAAT/enhancer-binding protein required for transcriptional activation of the serum albumin gene. *Genes Dev*. 1990;4(8):1416-1426.
- Landschulz WH, Johnson PF, McKnight SL. The DNA binding domain of the rat liver nuclear protein C/EBP is bipartite. *Science*. 1989;243(4899):1681-1688.
- Nerlov C, Ziff EB. CCAAT/enhancer binding protein-alpha amino acid motifs with dual TBP and TFIIIB binding ability co-operate to activate transcription in both yeast and mammalian cells. *Embo J*. 1995;14(17):4318-4328.
- Lin FT, MacDougall OA, Diehl AM, Lane MD. A 30-kDa alternative translation product of the CCAAT/enhancer binding protein alpha message:

- transcriptional activator lacking antimitotic activity. *Proc Natl Acad Sci U S A*. 1993;90(20):9606-9610.
7. Calkhoven CF, Muller C, Leutz A. Translational control of C/EBP α and C/EBP β isoform expression. *Genes Dev*. 2000;14(15):1920-1932.
 8. Pabst T, Mueller BU, Zhang P, et al. Dominant-negative mutations of CEBPA, encoding CCAAT/enhancer binding protein- α (C/EBP α), in acute myeloid leukemia. *Nat Genet*. 2001;27(3):263-270.
 9. Radomska HS, Huettner CS, Zhang P, Cheng T, Scadden DT, Tenen DG. CCAAT/enhancer binding protein α is a regulatory switch sufficient for induction of granulocytic development from bipotential myeloid progenitors. *Mol Cell Biol*. 1998;18(7):4301-4314.
 10. Christy RJ, Yang VW, Ntambi JM, et al. Differentiation-induced gene expression in 3T3-L1 preadipocytes: CCAAT/enhancer binding protein interacts with and activates the promoters of two adipocyte-specific genes. *Genes Dev*. 1989;3(9):1323-1335.
 11. McNagny KM, Sieweke MH, Doderlein G, Graf T, Nerlov C. Regulation of eosinophil-specific gene expression by a C/EBP-Ets complex and GATA-1. *Embo J*. 1998;17(13):3669-3680.
 12. Umek RM, Friedman AD, McKnight SL. CCAAT-enhancer binding protein: a component of a differentiation switch. *Science*. 1991;251(4991):288-292.
 13. Slomiany BA, D'Arigo KL, Kelly MM, Kurtz DT. C/EBP α inhibits cell growth via direct repression of E2F-DP-mediated transcription. *Mol Cell Biol*. 2000;20(16):5986-5997.
 14. Porse BT, Bryder D, Theilgaard-Monch K, et al. Loss of C/EBP α cell cycle control increases myeloid progenitor proliferation and transforms the neutrophil granulocyte lineage. *J Exp Med*. 2005;202(1):85-96.
 15. Porse BT, Pedersen TA, Xu X, et al. E2F repression by C/EBP α is required for adipogenesis and granulopoiesis in vivo. *Cell*. 2001;107(2):247-258.
 16. Zada AA, Pulikkan JA, Bararia D, et al. Proteomic discovery of Max as a novel interacting partner of C/EBP α : a Myc/Max/Mad link. *Leukemia*. 2006;20(12):2137-2146.
 17. Pedersen TA, Kowenz-Leutz E, Leutz A, Nerlov C. Cooperation between C/EBP α TBP/TFIIB and SWI/SNF recruiting domains is required for adipocyte differentiation. *Genes Dev*. 2001;15(23):3208-3216.
 18. Johansen LM, Iwama A, Lodie TA, et al. c-Myc is a critical target for c/EBP α in granulopoiesis. *Mol Cell Biol*. 2001;21(11):3789-3806.
 19. D'Alo F, Johansen LM, Nelson EA, et al. The amino terminal and E2F interaction domains are critical for C/EBP α -mediated induction of granulopoietic development of hematopoietic cells. *Blood*. 2003;102(9):3163-3171.
 20. Gombart AF, Hofmann WK, Kawano S, et al. Mutations in the gene encoding the transcription factor CCAAT/enhancer binding protein α in myelodysplastic syndromes and acute myeloid leukemias. *Blood*. 2002;99(4):1332-1340.
 21. Snaddon J, Smith ML, Neat M, et al. Mutations of CEBPA in acute myeloid leukemia FAB types M1 and M2. *Genes Chromosomes Cancer*. 2003;37(1):72-78.
 22. Renneville A, Boissel N, Gachard N, et al. The favorable impact of CEBPA mutations in patients with acute myeloid leukemia is only observed in the absence of associated cytogenetic abnormalities and FLT3 internal duplication. *Blood*. 2009;113(21):5090-5093.
 23. Leroy H, Roumier C, Huyghe P, Biggio V, Fenaux P, Preudhomme C. CEBPA point mutations in hematological malignancies. *Leukemia*. 2005;19(3):329-334.
 24. Shih LY, Liang DC, Huang CF, et al. AML patients with CEBP α mutations mostly retain identical mutant patterns but frequently change in allelic distribution at relapse: a comparative analysis on paired diagnosis and relapse samples. *Leukemia*. 2006;20(4):604-609.
 25. Preudhomme C, Sagot C, Boissel N, et al. Favorable prognostic significance of CEBPA mutations in patients with de novo acute myeloid leukemia: a study from the Acute Leukemia French Association (ALFA). *Blood*. 2002;100(8):2717-2723.
 26. Wouters BJ, Lowenberg B, Erpelink-Verschueren CA, van Putten WL, Valk PJ, Delwel R. Double CEBPA mutations, but not single CEBPA mutations, define a subgroup of acute myeloid leukemia with a distinctive gene expression profile that is uniquely associated with a favorable outcome. *Blood*. 2009;113(13):3088-3091.
 27. Fuchs O, Provaznikova D, Kocova M, et al. CEBPA polymorphisms and mutations in patients with acute myeloid leukemia, myelodysplastic syndrome, multiple myeloma and non-Hodgkin's lymphoma. *Blood Cells Mol Dis*. 2008;40(3):401-405.
 28. Shih LY, Huang CF, Lin TL, et al. Heterogeneous patterns of CEBP α mutation status in the progression of myelodysplastic syndrome and chronic myelomonocytic leukemia to acute myelogenous leukemia. *Clin Cancer Res*. 2005;11(5):1821-1826.
 29. Kirstetter P, Schuster MB, Bereshchenko O, et al. Modeling of C/EBP α mutant acute myeloid leukemia reveals a common expression signature of committed myeloid leukemia-initiating cells. *Cancer Cell*. 2008;13(4):299-310.
 30. Bereshchenko O, Mancini E, Moore S, et al. Hematopoietic stem cell expansion precedes the generation of committed myeloid leukemia-initiating cells in C/EBP α mutant AML. *Cancer Cell*. 2009;16(5):390-400.
 31. Dash A, Gilliland DG. Molecular genetics of acute myeloid leukaemia. *Best Pract Res Clin Haematol*. 2001;14(1):49-64.
 32. Renneville A, Roumier C, Biggio V, et al. Cooperating gene mutations in acute myeloid leukemia: a review of the literature. *Leukemia*. 2008;22(5):915-931.
 33. Kottaridis PD, Gale RE, Frew ME, et al. The presence of a FLT3 internal tandem duplication in patients with acute myeloid leukemia (AML) adds important prognostic information to cytogenetic risk group and response to the first cycle of chemotherapy: analysis of 854 patients from the United Kingdom Medical Research Council AML 10 and 12 trials. *Blood*. 2001;98(6):1752-1759.
 34. Beghini A, Ripamonti CB, Cairoli R, et al. KIT activating mutations: incidence in adult and pediatric acute myeloid leukemia, and identification of an internal tandem duplication. *Haematologica*. 2004;89(8):920-925.
 35. Ono R, Nakajima H, Ozaki K, et al. Dimerization of MLL fusion proteins and FLT3 activation synergize to induce multiple-lineage leukemogenesis. *J Clin Invest*. 2005;115(4):919-929.
 36. Kelly LM, Kutok JL, Williams IR, et al. PML/RAR α and FLT3-ITD induce an APL-like disease in a mouse model. *Proc Natl Acad Sci U S A*. 2002;99(12):8283-8288.
 37. Ding Y, Harada Y, Imagawa J, Kimura A, Harada H. AML1/RUNX1 point mutation possibly promotes leukemic transformation in myeloproliferative neoplasms. *Blood*. 2009;114(25):5201-5205.
 38. Yokota S, Kiyoi H, Nakao M, et al. Internal tandem duplication of the FLT3 gene is preferentially seen in acute myeloid leukemia and myelodysplastic syndrome among various hematological malignancies. A study on a large series of patients and cell lines. *Leukemia*. 1997;11(10):1605-1609.
 39. Murata K, Kumagai H, Kawashima T, et al. Selective cytotoxic mechanism of GTP-14564, a novel tyrosine kinase inhibitor in leukemia cells expressing a constitutively active Fms-like tyrosine kinase 3 (FLT3). *J Biol Chem*. 2003;278(35):32892-32898.
 40. Watanabe-Okochi N, Kitaura J, Ono R, et al. AML1 mutations induced MDS and MDS/AML in a mouse BMT model. *Blood*. 2008;111(8):4297-4308.
 41. Morita S, Kojima T, Kitamura T. Plat-E: an efficient and stable system for transient packaging of retroviruses. *Gene Ther*. 2000;7(12):1063-1066.
 42. Kitamura T, Koshino Y, Shibata F, et al. Retrovirus-mediated gene transfer and expression cloning: powerful tools in functional genomics. *Exp Hematol*. 2003;31(11):1007-1014.
 43. Lu Y, Kitaura J, Oki T, et al. Identification of TSC-22 as a potential tumor suppressor that is upregulated by Flt3-D835V but not Flt3-ITD. *Leukemia*. 2007;21(11):2246-2257.
 44. Fukuchi Y, Shibata F, Ito M, et al. Comprehensive analysis of myeloid lineage conversion using mice expressing an inducible form of C/EBP α . *EMBO J*. 2006;25(14):3398-3410.
 45. Cleaves R, Wang QF, Friedman AD. C/EBP α ph30, a myeloid leukemia oncoprotein, limits G-CSF receptor expression but not terminal granulopoiesis via site-selective inhibition of C/EBP DNA binding. *Oncogene*. 2004;23(3):716-725.
 46. Wang QF, Friedman AD. CCAAT/enhancer-binding proteins are required for granulopoiesis independent of their induction of the granulocyte colony-stimulating factor receptor. *Blood*. 2002;99(8):2776-2785.
 47. Iwasaki M, Kuwata T, Yamazaki Y, et al. Identification of cooperative genes for NUP98-HOXA9 in myeloid leukemogenesis using a mouse model. *Blood*. 2005;105(2):784-793.
 48. Hasemann MS, Damgaard I, Schuster MB, et al. Mutation of C/EBP α predisposes to the development of myeloid leukemia in a retroviral insertional mutagenesis screen. *Blood*. 2008;111(8):4309-21.
 49. Nakajima H, Shibata F, Kumagai H, Shimoda K, Kitamura T. Tyk2 is dispensable for induction of myeloproliferative disease by mutant FLT3. *Int J Hematol*. 2006;84(1):54-59.
 50. Reddy VA, Iwama A, Iotzova G, et al. Granulocyte inducer C/EBP α inactivates the myeloid master regulator PU. 1: possible role in lineage commitment decisions. *Blood*. 2002;100(2):483-490.
 51. Schwieger M, Löhler J, Fischer M, Herwig U, Tenen DG, Stocking C. A dominant-negative mutant of C/EBP α , associated with acute myeloid leukemias, inhibits differentiation of myeloid and erythroid progenitors of man but not mouse. *Blood*. 2004;103(7):2744-2752.
 52. Iwama A, Osawa M, Hirasawa R, et al. Reciprocal roles for CCAAT/enhancer binding protein (C/EBP) and PU. 1 transcription factors in Langerhans cell commitment. *J Exp Med*. 2002;195(5):547-558.
 53. Nerlov C. C/EBP α mutations in acute myeloid leukaemias. *Nat Rev Cancer*. 2004;4(5):394-400.
 54. Schuster MB, Porse BT. C/EBP α : a tumour suppressor in multiple tissues? *Biochim Biophys Acta*. 2006;1766(1):88-103.

miR-493 induction during carcinogenesis blocks metastatic settlement of colon cancer cells in liver

Koji Okamoto^{1,*}, Tatsuya Ishiguro¹, Yutaka Midorikawa², Hirokazu Ohata¹, Masashi Izumiya³, Naoto Tsuchiya³, Ai Sato¹, Hiroaki Sakai¹ and Hitoshi Nakagama^{3,*}

¹Division of Cancer Differentiation, National Cancer Center Research Institute, Tokyo, Japan, ²Teikyo University School of Medicine University Hospital, Kawasaki, Japan and ³Division of Cancer Development System, National Cancer Center Research Institute, Tokyo, Japan

Liver metastasis is a major lethal complication associated with colon cancer, and post-intravasation steps of the metastasis are important for its clinical intervention. In order to identify inhibitory microRNAs (miRNAs) for these steps, we performed 'dropout' screens of a miRNA library in a mouse model of liver metastasis. Functional analyses showed that miR-493 and to a lesser extent miR-493* were capable of inhibiting liver metastasis. miR-493 inhibited retention of metastasized cells in liver parenchyma and induced their cell death. IGF1R was identified as a direct target of miR-493, and its inhibition partially phenocopied the anti-metastatic effects. High levels of miR-493 and miR-493*, but not pri-miR-493, in primary colon cancer were inversely related to the presence of liver metastasis, and attributed to an increase of miR-493 expression during carcinogenesis. We propose that, in a subset of colon cancer, upregulation of miR-493 during carcinogenesis prevents liver metastasis via the induction of cell death of metastasized cells.

The EMBO Journal (2012) 0, 000–000

doi:10.1038/emboj.2012.25

Subject Categories: RNA; molecular biology of disease

Keywords: colon cancer; IGF-1R; metastasis; miR-493

Introduction

Colon cancer is the second leading cause of cancer-related death in the western world, and the third in the entire world (<http://globocan.iarc.fr/>). A major cause of the lethality of colon cancer is distant metastasis, especially metastasis to the liver, which is found in ~60% of colon cancer patients (Hess *et al*, 2006). In spite of recent progress, overall curative effects of chemotherapy, radiotherapy, and liver surgery for liver metastasis are dismal, resulting in a high rate of lethality for patients (Cunningham *et al*, 2010).

*Corresponding author. K Okamoto, Division of Cancer Differentiation, National Cancer Center Research Institute, 5-1-1 Tsukiji, Chuo-ku, Tokyo 104-0045, Japan. Tel.: +81 3 3542 2511; Fax: +81 3 3542 2980; E-mail: kojokamo@ncc.go.jp or H Nakagama, Division of Cancer Development System, National Cancer Center Research Institute, 5-1-1 Tsukiji, Chuo-ku, Tokyo 104-0045, Japan. E-mail: hnakagam@ncc.go.jp

Received: 1 September 2011; accepted: 18 January 2012

The development of liver metastasis of colon cancer is, like many other types of cancer metastasis, the result of a sequence of events that cancer cells pass through successfully (Gupta and Massagué, 2006; Chaffer and Weinberg, 2011). First, tumour cells acquire motility through a transforming process called epithelial mesenchymal transition (EMT), and break through the basement membrane into surrounding tissues. Second, the transformed cells intravasate local blood vessels that lead to a major portal vein, and survive in the blood stream. Third, the survived cells settle in liver parenchyma. Finally, cancer cells that settle in a new environment restart proliferation to form a metastatic foci.

For successful formation of metastatic foci in the liver, the final two steps of metastasis seem challenging, because the cells must adapt to the harsh microenvironment of the liver. On the other hand, the former steps seem relatively easy to be overcome due to direct blood circulation via portal veins and the porous nature of liver sinusoids (Chambers *et al*, 2002). Thus, the biological mechanisms by which the metastatic cells settle and proliferate in liver parenchyma are of particular interest for clinical intervention (Shibue and Weinberg, 2011).

In spite of the potential importance of the regulation of metastasis, our knowledge of the regulatory mechanism of the settlement and proliferation of metastatic cells in the liver is still limited. It is unclear which gene or network of genes plays a regulatory role in determining whether cancer cells successfully settle and grow in the liver. This is partly due to difficulties in setting up an appropriate *in vitro* system in which the effects of potential regulatory genes on metastatic cells can be evaluated. Without such a system, it is difficult to systematically search for functional regulators of tumour proliferation in the liver. Systematic screening of such regulators in experimental animals *in vivo* is an alternative, but such an attempt has not been reported, probably due to associated technical difficulties.

Accumulating reports have firmly established microRNAs (miRNAs) as one of the central players that regulate many aspects of cancer progression, including regulation of metastasis (Lotterman *et al*, 2008; Dumont and Tlsty, 2009; Iorio and Croce, 2009; Nicoloso *et al*, 2009; Ventura and Jacks, 2009). miRNA is ~22 nt RNA in its mature form, and produced from its precursor mRNA (pri-miRNA) after sequential processing (Winter *et al*, 2009). Mature miRNA, by forming a RISC complex with other associated proteins, inhibits its downstream target genes by regulating mRNA stability and translation of their products (Bartel, 2009; Winter *et al*, 2009).

Like other types of cancer, many miRNAs are differentially regulated during the development of colon cancer (Dong *et al*, 2011), and some have been shown to play regulatory roles. While most of such regulatory miRNAs are involved in cell proliferation and apoptosis of colon cancer, some are involved in the regulation of metastasis. For example, miR-21, miR-26, miR-31, miR-141, miR-145, miR-196, and miR-200

were shown to be associated with the migration/invasiveness of colon cancer, miR-107 with angiogenesis, and the miR-200 family with stem cell-like properties (de Krijger *et al*, 2011; Wu *et al*, 2011). However, the phenotypes of these regulatory miRNAs were, in general, linked to the early stages of metastasis, and no miRNA has been identified that is clearly responsible for the last stages, that is, settlement or proliferation of metastasized cells in the liver or other distant target organs.

In order to identify regulatory miRNAs that inhibit these post-intravasation steps of liver metastasis, we performed a functional screening of miRNAs that inhibit the metastasis of colon cancer cells under experimental settings that reflect the final metastatic processes. Because 'dropout' assays have been successfully used to isolate genes and miRNAs that inhibit cell growth and the invasion of cancer cells (Voorhoeve *et al*, 2006; le Sage *et al*, 2007; Huang *et al*, 2008; Schlabach *et al*, 2008; Izumiya *et al*, 2011), we utilized the genetic power of dropout assays to isolate anti-metastatic miRNAs in a mouse model of liver metastasis. The following analyses revealed that miR-493 and miR-493* were capable of inhibiting the settlement of colon cancer cells in the liver parenchyma, at least in part by inducing their cell death. Possible roles of miR-493 in regulating liver metastasis, in light of their expression profiles in clinical specimens, are discussed.

Results

Functional screening for miRNAs that inhibit liver metastasis of colon cancer cells

We aimed to functionally isolate miRNAs that inhibit liver metastasis under experimental conditions in which the settlement of metastatic cells into the liver parenchyma via portal vein is reproduced (Figure 1A). We introduced a GFP-expressing lentivirus library that expresses miRNA precursors from mini-miRNA genes (a mixture of 445 human miRNAs) into HCT116 colon cancer cells, and a pool of the library-introduced cells was injected into the spleen of immunocompromised NOG mice. Two weeks after the injection, the development of liver metastasis was observed as multiple GFP-positive foci on liver surfaces while a fraction of the cells proliferated in the inoculated spleen (Figure 1B). GFP expression in the cancer cells allowed us to visualize the process of liver metastasis as reported previously (Wang *et al*, 2004).

While metastatic foci were formed on liver surfaces (Figure 1B), GFP images (Figure 1C), and HE staining (Figure 1D) of liver sections revealed that they were also formed in the liver parenchyma. HE staining of metastasized liver at an early stage (day 5 after splenic injection) indicated that the metastasized foci were generally localized in the vicinity of E-cadherin-positive areas surrounding the portal triads (Figure 1E). These data and previous reports (Bouvet *et al*, 2006) indicate that the generated metastasis was indeed disseminated through a portal vein after splenic injection.

In order to isolate miRNAs that inhibit liver metastasis, library-introduced cells were recovered from the spleen and liver 2 weeks after splenic injection, and DNA fragments of library miRNAs that were integrated into the genome of infected cells were amplified by PCR. Subsequently, the fragments were labelled either with Cy3 (miRNAs isolated from spleen) or with Cy5 (miRNAs isolated from liver),

and used for two-colour microarray analyses in order to quantify the Cy5/Cy3 ratio of each library miRNA. This 'dropout' screen has been successfully employed by other groups (Voorhoeve *et al*, 2006; Huang *et al*, 2008; Schlabach *et al*, 2008) as well as in our previous studies (Izumiya *et al*, 2010; Tsuchiya *et al*, 2011) to isolate genes that inhibit cell proliferation. We repeated the screening four times (the dropout assays were performed with the genomic DNA isolated from the two independently injected mice in duplicate), and identified 25 miRNAs whose expression induced >10-fold reduction of the Cy5/Cy3 ratios on average (Supplementary Table S1; Figure 1F). Of the 25 miRNAs, 7 miRNAs (miR-128a, miR-668, miR-657, miR-493, miR-583, miR-659, and miR-125b) induced statistically significant reduction ($P < 0.01$) of the Cy5/Cy3 ratios (Figure 1F).

miR-493 expression inhibits liver metastasis of colon cancer cells

In order to quantitatively determine if the candidate miRNAs identified by screening inhibit liver metastasis, HCT116 cells were individually infected with GFP-expressing lentiviruses that express the corresponding miRNA precursor, mixed with cells infected with RFP-expressing lentiviruses (HCT116/RFP) at a 1:1 ratio, and injected into the spleen of NOG mice to generate liver metastasis (Figure 2A). Two weeks after injection, the extent of inhibition of liver metastasis was examined by evaluating the ratios of the number of GFP- or RFP-positive cells from metastasized liver by GFP/RFP dual imaging of metastatic foci (Figure 2C) or by quantification of GFP- and RFP-positive cells by flow cytometry (Figure 2B). We speculated that two types of miRNAs are selected after the screening; miRNAs that inhibit attachment or proliferation of the cancer cells in the liver, and those that induce them in the spleen. This validation step should identify miRNAs that belong to the former, and eliminate the latter.

GFP/RFP dual imaging showed that the formation of GFP-positive foci was markedly inhibited by introducing the viruses that expressed precursors of miR-493, or miR-125b, while the formation of RFP-positive foci was not significantly affected in either case (Figure 2C), indicating that these miRNAs inhibited formation of the metastatic foci in the liver. The other candidate miRNAs did not cause apparent inhibition of GFP foci (Figure 2B and unpublished results). In accordance with these observations, quantification of the ratios of a number of GFP- and RFP-positive metastasized cells demonstrated that miR-493 expression caused the strongest inhibition of liver metastasis while miR-125b and let-7e also showed significant inhibition (Figure 2B). Proliferation of miRNA-introduced cells *in vitro* under normal culture conditions revealed that the expression of miR-125b or let-7e, but not miR-493, apparently inhibited cell growth (Supplementary Figure S1A), indicating that the inhibitory effects of miR-125b and let-7e may be mainly caused by general inhibition of cell growth. Therefore, we focused on analysing miR-493 functions in the following studies.

From the miR-493 precursor introduced by the lentiviruses, a minor starform of miR-493 (miR-493*) as well as authentic miR-493 can be produced. In fact, examination of miRNA expression revealed that both forms of miRNAs were expressed in the infected HCT116 (Figure 2E). Examination of the levels of endogenous miR-493 and miR-493* by RT-qPCR indicated that neither form of miRNA was expressed in any

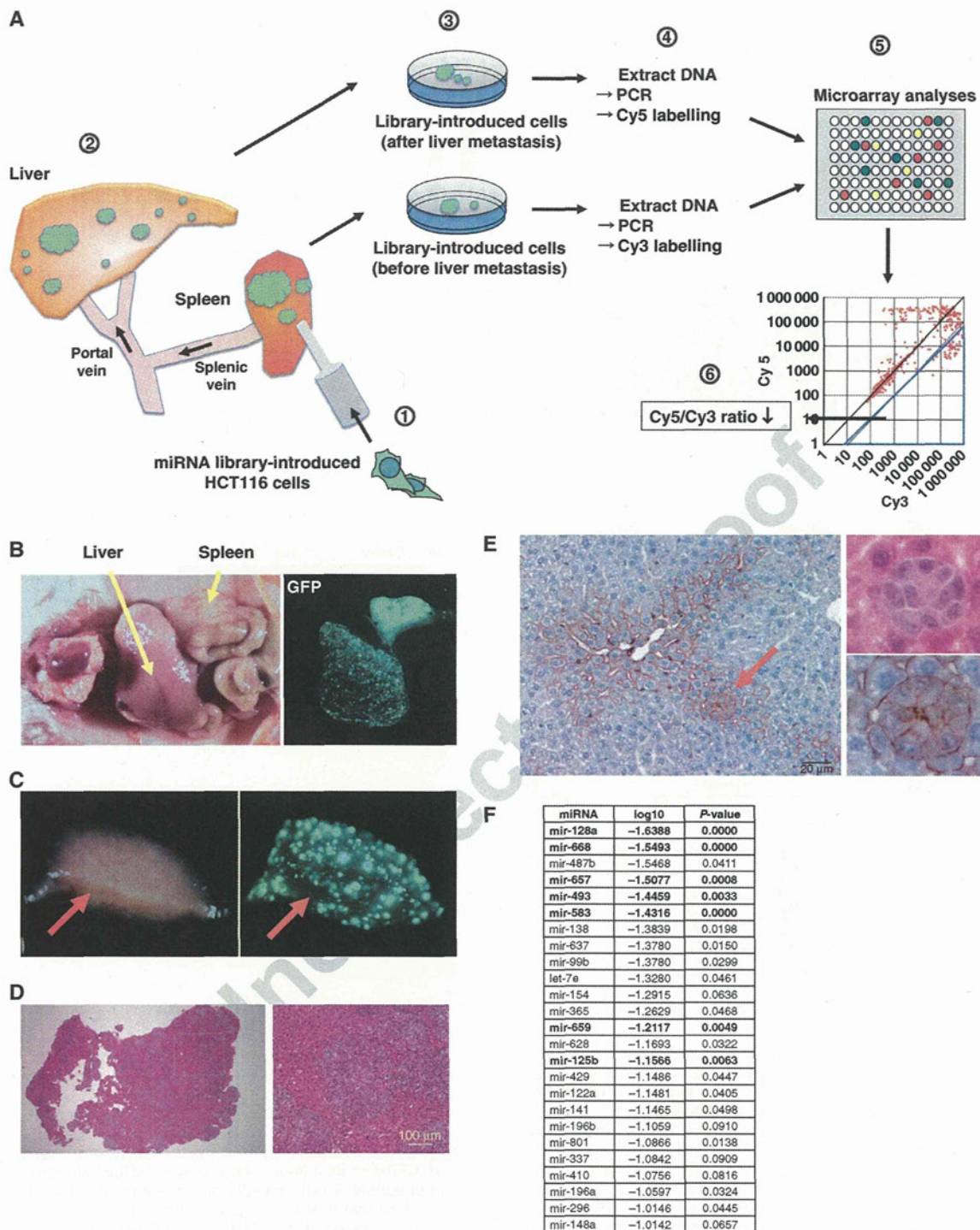


Figure 1 Functional screening for miRNAs that inhibit liver metastasis of colon cancer cells. (A) Schematic for functional screening of miRNAs that inhibit liver metastasis of colon cancer cells. (1) HCT116 cells that were infected with a human miRNA lentivirus library were injected into the spleens of NOG mice. (2, 3) Two weeks after the injection, library-introduced cells were recovered from the spleen and liver, and used to isolate genomic DNA. (4, 5) The introduced miRNA was amplified from the genomic DNA by PCR, labelled with Cy3 (spleen) or Cy5 (liver), and the Cy5/Cy3 ratio of each library-introduced miRNA was determined with the custom-made microarray (see Materials and methods). (6) miRNAs with low Cy5/Cy3 values were regarded as positive 'dropout' clones. (B) Bright-phase (left) and GFP (right) images of metastasized liver (2 weeks after splenic injection). (C) Bright-phase (left) and GFP (right) images of the metastasized liver at higher magnification. Arrow shows cut surface. (D) HE section of the metastasized liver (2 weeks after splenic injection). (E) Immunostaining of the metastasized liver (5 days after splenic injection). The metastasized liver was immunostained with E-cadherin (left and lower right), or stained with HE (upper right). The right panels show magnified images. Arrow indicates a metastasized HCT116 focus. (F) A list of 'dropout' clones with low Cy5/Cy3 ratio (>10-fold). miRNAs with low *P*-values (*P*<0.01) are shown in bold. *P*-values were calculated by standardizing each of the four experimental data sets by *Z*-score transformation and then by examining null hypothesis that the dropout value of certain miRNA is identical to the average of dropout values of all miRNAs in the library. Welch's *t*-test was performed to calculate *P*-value.

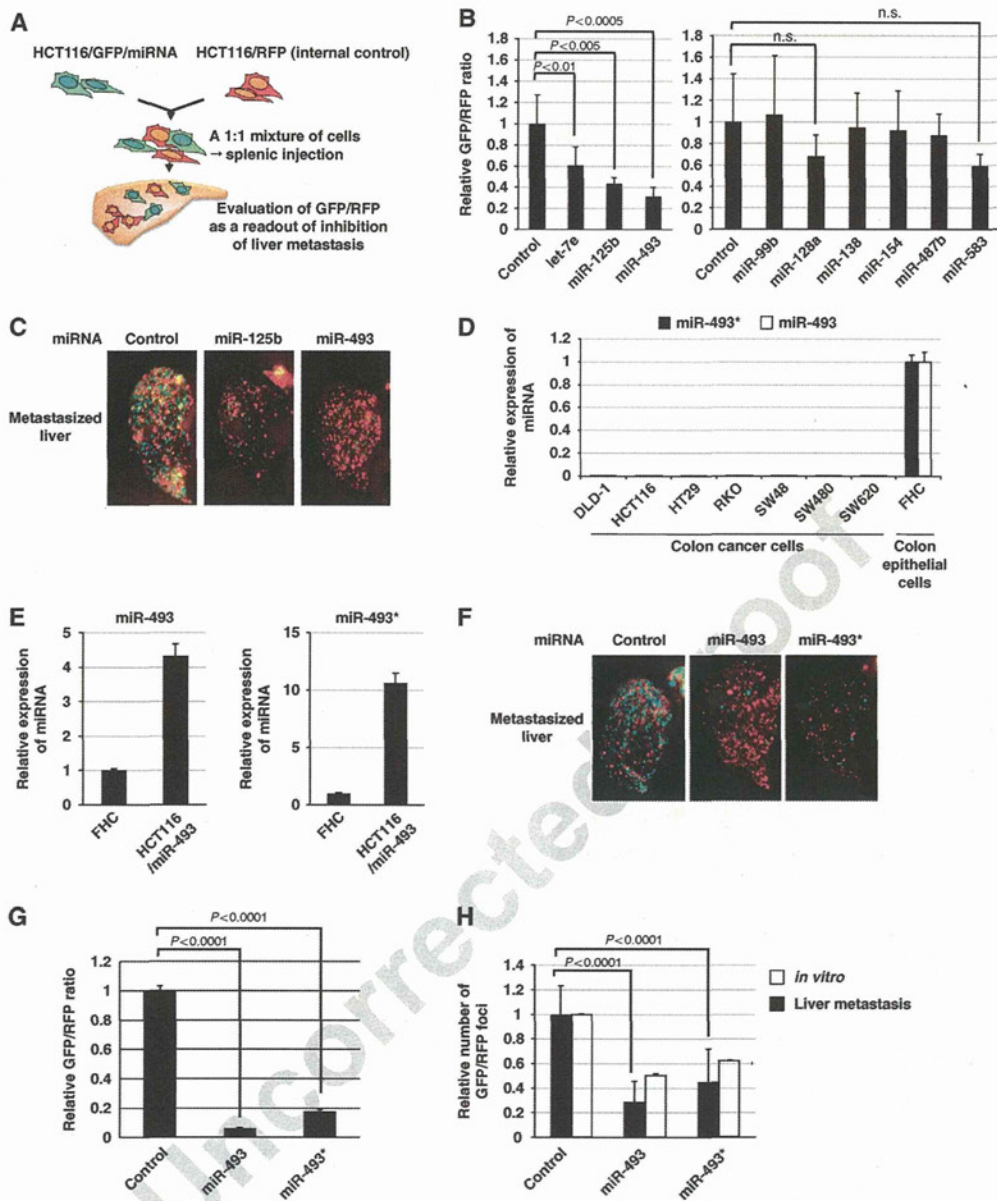


Figure 2 miR-493 expression inhibits liver metastasis of colon cancer cells. (A) Schematic for evaluation of inhibitory effects of each miRNA on liver metastasis. HCT116/GFP cells introduced with individual miRNA were mixed with HCT116/RFP cells at a 1:1 ratio, and the mixture was used for splenic injection to generate liver metastasis. (B, C) Inhibition of liver metastasis by miRNA precursors. HCT116/GFP cells were infected with the lentiviruses that express the indicated miRNA precursors, and the mixtures of the infected HCT116/GFP cells and HCT116/RFP cells were used for the splenic injection. (B) Metastasized cells were isolated from the liver 14 days after the splenic injection, and a number of GFP-positive and RFP-positive cells were counted by flow cytometry. The inhibitory effect of each miRNA was evaluated by calculating GFP/RFP ratio. (C) Inhibition of liver metastasis by miRNAs (day 14). GFP/RFP dual fluorescence images for the indicated miRNA precursors were taken. (D) miR-493 expression in colon cancer cells and colon epithelial cells. miR-493 and miR-493* expression of the indicated cells was determined by RT-qPCR. (E) RT-qPCR analyses of miR-493 (left) and miR-493* (right) in FHC cells and HCT116 cells infected with the lentiviruses that express the miR-493 precursor. (F) Inhibition of liver metastasis by miR-493 and miR-493* mimics. GFP/RFP dual fluorescence images for the indicated miRNAs were taken as described in (C). (G) Inhibition of liver metastasis by miR-493 and miR-493* mimics. Inhibitory effect of each miRNA was evaluated as described in (B). (H) Inhibitory effect of miR-493 and miR-493* mimics in DLD-1 cells. For liver metastasis assays, the inhibitory effect was evaluated by counting the number of GFP/RFP fluorescent foci 14 days after the splenic injection. For *in vitro* growth assays, the same mixture of cells was grown under normal culture condition for 14 days, and the GFP/RFP ratios were calculated by flow cytometry.

colon cancer cells examined, while they were expressed in FHC, normal colon epithelial cells (Figure 2D). The levels of miR-493 and miR-493* in FHC cells approximately correspond to 25 and 10% of those of the infected HCT116 cells (Figure 2E).

In order to determine which miRNA, miR-493 or miR-493*, was responsible for the inhibitory effect on liver metastasis, we transfected miRNA mimics of each form into GFP-expressing HCT116 cells (HCT116/GFP), and their inhibitory effects on liver metastasis were examined in liver metastasis assays.

Interestingly, both forms of miRNA were capable of inhibiting liver metastasis (Figure 2F and G), and miR-493 and miR-493* caused ~20-fold and ~5-fold reduction of the GFP/RFP ratio, respectively (Figure 2G). In contrast, miR-493 and miR-493* caused only an ~2.6-fold and ~2.1-fold reduction of the ratio in cells that proliferated in spleen (Supplementary Figure S1B). Likewise, growth of cells transfected with miRNA mimics *in vitro* under normal culture conditions showed that introduction of miR-493 or miR-493* caused only an ~2.5-fold reduction of GFP/RFP ratios (Supplementary Figure S1C). These results suggest that the inhibitory function of the miRNAs cannot be attributed to mere inhibition of cell growth and are at least in part associated with liver metastasis.

We also examined the inhibitory effects of miR-493 on DLD-1, another colon cancer cell line. DLD-1 cells were transfected with the miRNA mimics and used for the splenic injection. Because metastasized DLD-1 cells grow slowly and it is difficult to obtain a sufficient number of cells to quantify GFP/RFP ratio by flow cytometry (unpublished results), the number of foci was counted from the GFP/RFP dual image to evaluate their effects on liver metastasis. Introduction of miR-493 or miR-493* caused an ~4-fold or ~2.5-fold inhibition of liver metastasis, whereas both caused an ~2-fold inhibition of the GFP/RFP ratios under normal culture conditions (Figure 2H). Thus, miR-493 and to a lesser extent miR-493* were capable of inhibiting liver metastasis in at least two different colon cancer cell lines.

miR-493 expression induces cell death of colon cancer cells in metastasized liver

Next, we attempted to determine the mechanisms by which miR-493 or miR-493* inhibits liver metastasis. In order to determine whether the inhibitory effects of miR-493 can be observed during early phases of the experiments, we examined GFP/RFP dual images 2 and 4 days after splenic injection. Evaluation of GFP/RFP ratios indicated that miR-493 expression did not significantly affect liver metastasis on day 2, but caused marked inhibition on day 4 (Figure 3A and B). HE staining of metastasized liver indicated that the transfected HCT116/GFP cells were found in liver parenchyma 2 days after the splenic injection (Supplementary Figure S2A). Combined with the data presented in Figure 3A and B, these results indicate that miR-493 induced reduction of metastatic cells that already entered liver parenchyma.

In order to determine whether the marked reduction of GFP-positive foci by miR-493 on day 4 was caused by accelerated cell death in the liver parenchyma, Alexa 488-labelled Annexin V was injected via the tail vein on day 3 after the splenic injection of miRNA-transfected HCT116/RFP. Evaluation of a fraction of Annexin V-positive cells indicated that miR-493 markedly stimulates the induction of cell death of metastatic cells (Figure 3C). Thus, it is likely that the induction of cell death contributes to the inhibition of liver metastasis by miR-493.

Unexpectedly, transfection of miR-493* caused moderate induction of cell death (Figure 3C), although the GFP/RFP

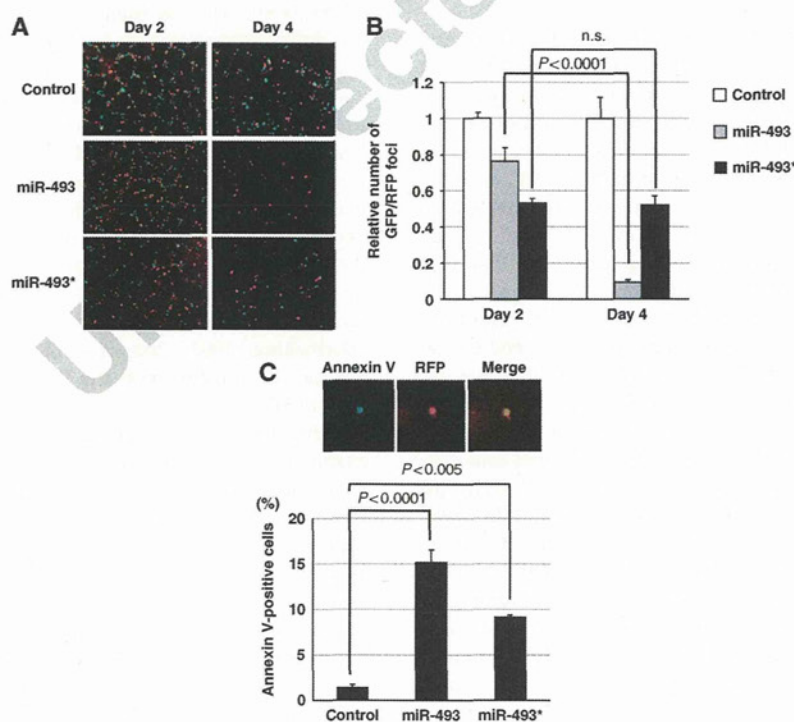


Figure 3 miR-493 expression induces cell death of colon cancer cells in metastasized liver. (A) GFP/RFP dual fluorescence images (higher magnification) of metastasized liver at day 2 or day 4 after splenic injection. HCT116/GFP cells were transfected with the indicated miRNA, and used for splenic injection as described in Figure 2C. (B) A number of GFP-positive and RFP-positive foci in (A) were counted and the relative ratio of GFP/RFP foci was calculated in each experiment. (C) Annexin V assays of metastasized cells transfected with miR-493. HCT116/RFP cells transfected with the indicated miRNA mimics were injected into the spleen. Three days after splenic injection, Alexa 488-Annexin V was injected via a tail vein, and the fraction of liver-metastasized HCT116/RFP cells that were positive for Annexin V staining was quantified under fluorescent microscope. Upper pictures show representative staining of HCT116/RFP cells with Alexa 488-Annexin V.

ratio did not significantly change between day 2 and day 4 (Figure 3B). Given that the number of RFP-positive foci was somewhat reduced when co-injected with miR-493*-transfected HCT116/GFP cells (Figure 2F), miR-493* may induce cell death not only in miR-493*-expressing cells but also in neighbouring metastatic cells in a cell non-autonomous manner.

In contrast to the marked increase of cell death in metastasized liver (Figure 3C), introduction of either miR-493 or miR-493* did not cause a significant increase of a fraction of Annexin V-positive cells *in vitro* under normal culture conditions (Supplementary Figure S2B). The lack of induction of cell death by miR-493 in *in vitro* condition was further supported by analyses of cells with a sub-G1 DNA content (data not shown). Thus, our data indicate that the induction of cell death by miR-493 is associated with liver metastasis.

IGF1R is a direct target of miR-493 and partially mediates the inhibition of liver metastasis by miR-493

In order to clarify the molecular mechanisms of miR-493-mediated inhibition of liver metastasis, we looked for its direct targets. We narrowed down the target genes by combining two criteria: (1) a combination of predicted targets from three *in-silico* programs (Targetscan, PITA, miRanda), (2) genes reduced by >2-fold after miRNA expression. Our functional analyses presented in Figure 2 suggest that miR-493* is less effective than miR-493 in inhibiting metastasis. In addition, predicted targets of miR-493* were not reported in two (Targetscan and PITA) out of the three programs. Therefore, we focused on identifying targets of miR-493 in the following studies.

A combination of the two criteria revealed that there are eight predicted targets whose expression was reduced by >2-fold after miR-493 expression (Figure 4A; Supplementary Table S2). Because miR-493 induces the cell death of metastasized cells (Figure 3C), IGF1R is of particular interest due to its known roles in cell survival and promotion of metastasis of various types of cancer, including colon cancer (Ewing and Goff, 2010). In fact, the introduction of miR-493 mimic or the infection with miR-493-expressing lentiviruses inhibited the expression of IGF1R, whereas other miRNAs, except miR-125b, did not suppress its expression (Figure 4B). The predicted target site for miR-493 is located near the 3' end of the 3' UTR of the *IGF1R* gene (Figure 4C). Functional luciferase assays indicated that the 3' UTR of *IGF1R* was repressed by miR-493, and mutation of the predicted target site completely abolished the repression (Figure 4D), indicating that miR-493 directly targets *IGF1R* for suppression via its 3' UTR. In contrast, other miRNAs (miR-493*, let-7e, miR-125b, miR-34a, miR-668) did not inhibit the same 3' UTR (Supplementary Figure S3A). Thus, inhibition of the 3' UTR of *IGF1R* by miR-493 is specific among miRNAs. Inhibition of *IGF1R* by miR-493 was also observed in DLD-1 (Figure 4E; Supplementary Figure S3B), indicating that miR-493 is capable of inhibiting *IGF1R* expression in at least two colon cancer cells.

In order to examine whether the repression of *IGF1R* mediates the anti-metastatic effects of miR-493, *IGF1R* expression was inhibited by transfection of corresponding siRNAs in HCT116/GFP (Figure 4F), and the transfected cells were used for functional analyses of liver metastasis as performed in Figure 2F. Inhibition of *IGF1R* caused 30–40%

reduction of liver metastasis (Figure 4G). Annexin V staining of the inhibited cells revealed that inhibition of *IGF1R* caused ~3-fold increase of cell death (Figure 4H). In order to determine whether *IGF1R* inhibition is required for miR-493-mediated suppression of metastasis, *IGF1R*-expressing lentiviruses were used to infect HCT116/GFP cells (Supplementary Figure S3C). *IGF1R* overexpression partially alleviated miR-493-mediated inhibition of liver metastasis (Supplementary Figure S3D). These data collectively indicated that *IGF1R* inhibition partly mediates the effects of miR-493 on the suppression of liver metastasis.

A high level of miR-493 expression is associated with the absence of liver metastasis of colon cancer

Given the observed roles of miR-493 in suppressing liver metastasis, we were interested in examining whether high levels of miR-493 expression in human colon cancer are associated with the absence of liver metastasis. Therefore, we measured the levels of miRNAs in surgical specimens from primary colon cancers by RT-qPCR assays. The 44 cases that were examined were classified into 3 groups; cases without liver metastasis (19 cases), with metachronous metastasis (12 cases), and with synchronous metastasis (13 cases). Among these groups, there was no significant difference ($P > 0.05$ by one-way ANOVA) in terms of age, gender, location, or size of tumours (Supplementary Table S3).

Average levels of miR-493 and miR-493* from primary cancer specimens without liver metastasis were ~2-fold and ~3-fold higher than those with synchronous metastasis, respectively, whereas their levels in specimens with metachronous metastasis were between those from the other two specimens (Figure 5A and B). Of note, none of the primary cancers with synchronous liver metastasis showed high levels of miR-493/miR-493* expression. It is unlikely that low levels of these miRNAs in primary tumours with liver metastasis were caused by alteration of the genomic loci because chromosomal loss of 14q32.2, the genomic region encompassing *miR-493*, was not commonly observed with these tumours by allelic copy number analyses (Izumiya *et al*, unpublished data). In contrast to miR-493 and miR-493*, levels of miR-34a, another tumour-suppressive miRNA (Hermeking, 2007; Tazawa *et al*, 2007), did not show an inverse relationship with the formation of liver metastasis (Figure 5C).

Using the same set of the tumour specimen, we also examined the expression of the six other miRNAs whose expression caused statistically significant inhibition of liver metastasis in the initial screening (Figure 1F). Because expression of miR-583 was not detectable in most of the samples, we analysed the remaining five miRNAs (miR-128a, miR-668, miR-657, miR-659, and miR-125b). Remarkably, none of these miRNAs showed the statistically significant differences among the three groups (Supplementary Figure S4A–E). These results indicated that the expression of miR-493/miR-493* was specifically elevated in a subset of primary tumours without liver metastasis, which is in agreement with their inhibitory roles in liver metastasis.

In contrast to liver metastasis, we did not observe significant reduction of levels of miR-493 or miR-493* in tumours with lung metastasis (Supplementary Figure S4F and G). Thus, the formation of liver metastasis is specifically

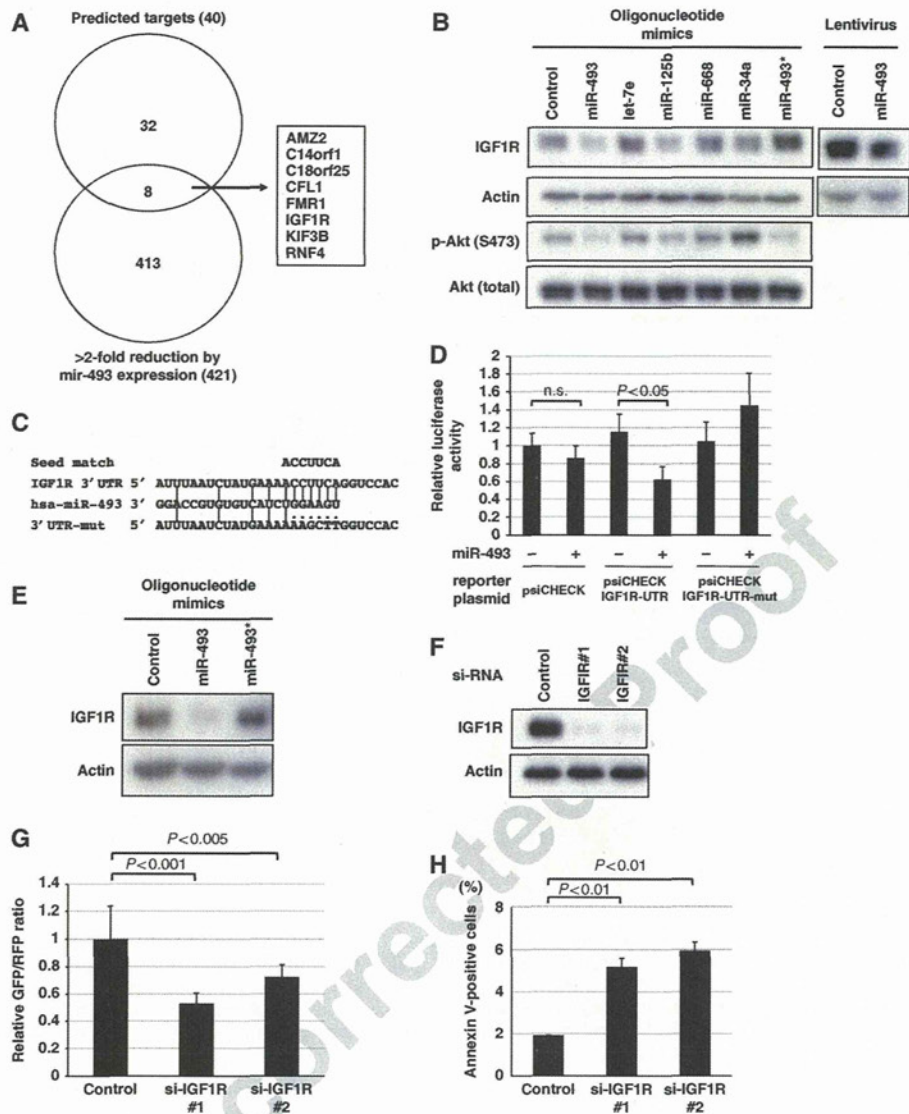


Figure 4 IGF1R is a direct target of miR-493 and partially mediates the inhibition of liver metastasis by miR-493. (A) Two-cycle Venn diagram shows the overlap of predicted target genes of miR-493 (40 genes) and genes inhibited by miR-493 expression (421 genes). (B) HCT116 cells were transfected with the indicated miRNA mimics (left panels), or infected with the control or the miR-493-expressing lentiviruses (right panels), and used for western blot analyses with the indicated antibodies. (C) Sequence comparison of IGF1R 3'UTR (positions 1311–1317), the mutated IGF1R 3'UTR, and human miR-493. (D) Transient luciferase assays. The indicated reporter plasmid was transfected into HCT116 cells together with control miRNA or miR-493 mimic, and luciferase activity was measured 2 days after transfection. (E) Western blot analyses in DLD-1 cells as shown in (B). (F) Western blot analyses in HCT116/GFP cells after transfection of control or the designated IGF1R siRNA. (G) Inhibition of liver metastasis by IGF1R siRNAs. The inhibitory effect of each siRNA was evaluated as described in Figure 2B. (H) Annexin V assays of metastasized HCT116 cells that were transfected with control or IGF1R siRNA. A fraction of Annexin V-positive cells after transfection of the indicated siRNA is shown as presented in Figure 3C.

associated with the reduced levels of these miRNAs in primary tumours.

In contrast to miR-493 and miR-493*, levels of their precursor (pri-miR-493) were not significantly altered among these specimens (Figure 5D). In fact, while levels of miR-493 and miR-493* were highly correlated (Pearson's correlation: $r=0.883$), neither was positively correlated with those of pri-miR-493 ($r=-0.303$ and $r=-0.168$, respectively) (Figure 5E). These results suggest that high levels of miR-493/miR-493* in a subset of cancer cells without liver metastasis were not caused by an increase of their precursor,

but by enhanced processing of the precursor into mature miRNAs.

Because IGF1R was inhibited by miR-493 (Figure 4), we examined whether expression of IGF1R is increased in primary cancers with liver metastasis. Immunostaining of IGF1R of the same primary tumour demonstrated that IGF1R was expressed at higher levels in tumours with synchronous metastasis than those without metastasis (Figure 5F), although inverse correlations between levels of IGF1R immunostaining and those of miR-493 or miR-493* were rather moderate ($r=-0.353$ and $r=-0.404$, respectively).

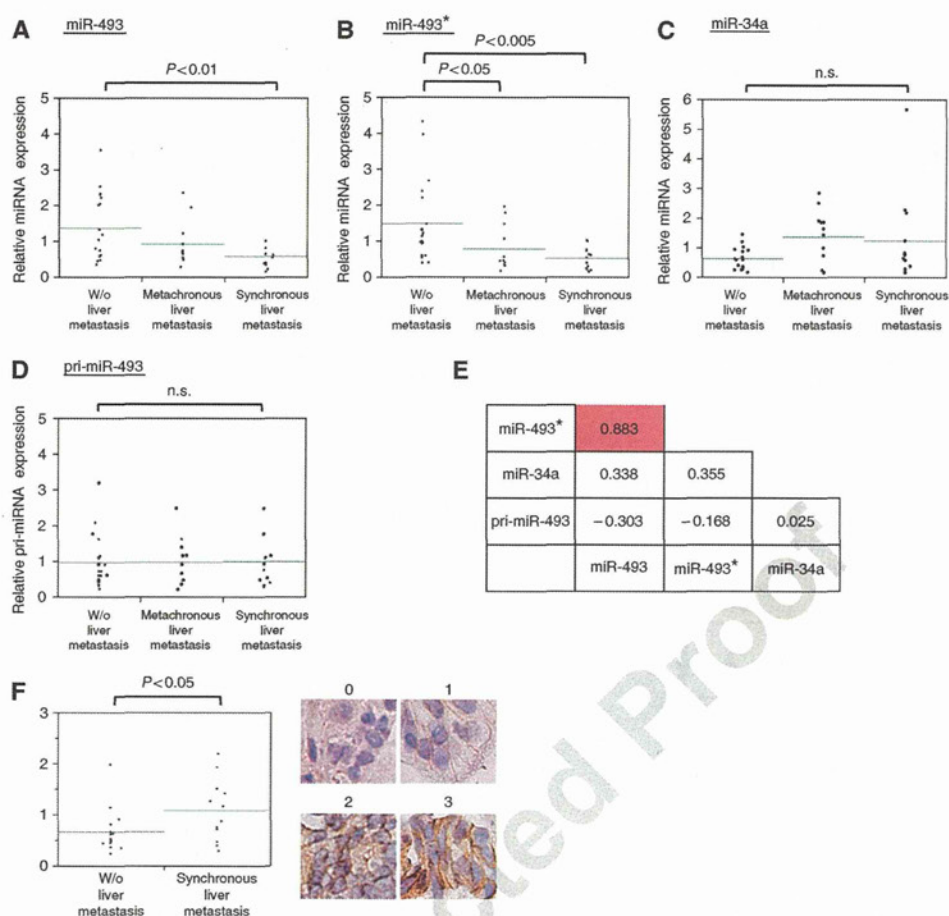


Figure 5 A high level of miR-493 expression is associated with the absence of liver metastasis of colon cancer. (A–D) RT–qPCR analyses of (A) miR-493, (B) miR-493*, (C) miR-34a, and (D) pri-miR-493 from the designated groups of primary colon tumours. Green lines indicate average values of each group. The relative miRNA expression level in each sample was normalized by the average of total samples. (E) Pearson's correlation coefficient between the designated variables. (F) Levels of IGF1R immunostaining of primary tumour without liver metastasis or with synchronous metastasis. Right panels indicate representative immunostaining from grade 0 to 3. Each immunostaining was quantified as described in Materials and methods.

Thus, the high levels of miR-493 may partly contribute to the reduced levels of IGF1R in tumours without liver metastasis.

miR-493 expression is induced during carcinogenesis in a subset of colon cancers

Finally, we examined whether miR-493/miR-493* expression is regulated during colon carcinogenesis using the same sets of tumours (without liver metastasis and synchronous metastasis) and corresponding non-tumour specimens. As demonstrated in Figure 5A and B, levels of miR-493 and miR-493* expressions were high in a subset of tumours without liver metastasis, and comparison of tumour and non-tumour specimens revealed that the high levels were attributed to their elevation during carcinogenesis (Figure 6A and C). On average, miR-493 and miR-493* were increased by ~2-fold and ~4-fold, respectively, during carcinogenesis of colon tumours without liver metastasis, whereas the induction of these miRNAs was significantly less in tumours with synchronous metastasis (Figure 6B and D). Thus, high levels of miR-493/miR-493* in a subset of tumours without liver metastasis are attributed to their induction during colon carcinogenesis.

In contrast to miR-493/miR-493*, the significant elevation of miR-34a or miR-125b was not observed during carcinogenesis of colon tumours without liver metastasis (~1.3-fold for miR-34a and ~1.2-fold for miR-125b; Supplementary Figure S5A–D). These data indicate that the increase of miR-493 during carcinogenesis in a subset of tumours with liver metastasis is unique among miRNAs.

Interestingly, miR-125b expression is apparently reduced during carcinogenesis of colon tumours with synchronous metastasis (~0.36-fold; Supplementary Figure S5C and D). Thus, given the inhibitory role of liver metastasis of miR-125b (Figure 2B), the reduction of miR-125b in colon tumour may also contribute to the generation of liver metastasis.

Discussion

A functional 'dropout' screen has been applied to identify genes and miRNAs that play inhibitory roles in cell proliferation or invasion of human cancer cells (Voorhoeve and Agami, 2007; Izumiya *et al*, 2011). Here, we extended its application for more complicated biological process, that is, regulation of liver metastasis. This was made possible by the

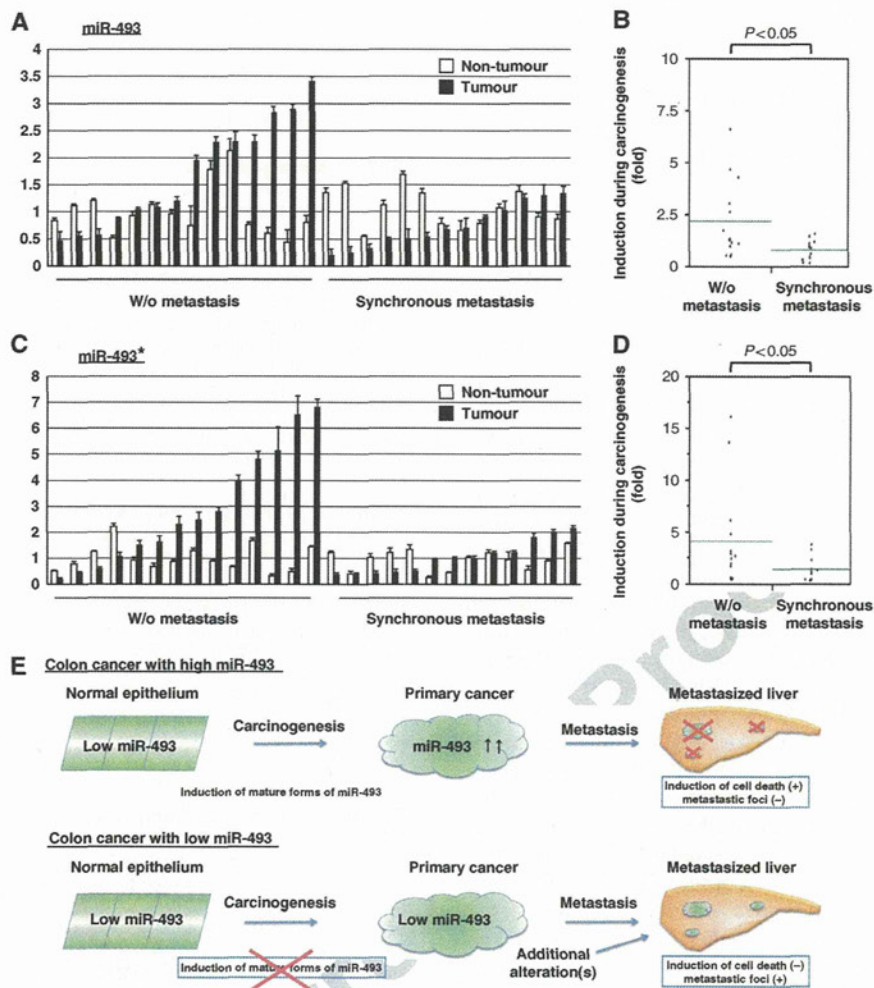


Figure 6 miR-493 expression is induced during carcinogenesis in a subset of colon cancers. (A, C) RT-qPCR analyses of (A) miR-493 and (C) miR-493* in 27 primary tumours (14 cases without liver metastasis and 13 cases with synchronous liver metastasis) and the corresponding non-cancerous specimens. (B, D) Ratios of (B) miR-493 and (D) miR-493* levels between tumour and non-cancerous specimens analysed in (A) and (C), respectively. (E) Model for the role of miR-493 in suppressing liver metastasis in a subset of liver tumours.

use of highly immunodeficient NOG mice that show high efficiency for the metastasis of human cells (Hamada *et al*, 2008), in combination with relatively small complexity of the library (445 miRNAs). In addition, use of RFP-positive cells as internal controls and measurement of GFP/RFP ratios as readouts for the inhibitory effect allowed us to quantitatively evaluate the effects of the identified miRNAs on liver metastasis. Presumably, a similar screening strategy will be applied to identify miRNAs, other types of non-coding RNAs, or shRNAs for a subset of genes, that can inhibit various types of distant metastasis in the future.

Through dropout screening using a mouse model of liver metastasis, we demonstrated that miR-493 induces the cell death of metastasized cells and inhibits liver metastasis of colon cancer cells. In addition, miR-493*, a starform miRNA that is derived from the same precursor, was also capable of inhibiting of liver metastasis. Expressions of two metastasis inhibitory miRNAs from the same precursor may co-operate to strengthen their inhibitory effects on liver metastasis.

An inverse correlation between miR-493 expression and the tendency to develop liver metastasis, considering its inhibitory roles against metastatic cells, strongly suggests that high levels of miR-493 prevent liver metastasis in human colon cancer. Remarkably, high levels of miR-493 expression in a subset of colon cancer were attributed to their induction during carcinogenesis. Hence, in some tumours, the induction of miR-493 during carcinogenesis may protect them from developing liver metastasis, while in others a lack of the induction may facilitate the formation of metastasis (Figure 6E).

The anti-metastatic functions of miR-493 are somewhat reminiscent of that of some known tumour suppressors, such as p53 (Vousden and Prives, 2009), which are activated in response to a variety of carcinogenic signals: carcinogenesis may trigger the induction of miR-493 in some colon cancers as one of cellular responses to prevent liver metastasis, although it is uncertain whether the induction functions to inhibit early stages of cancer development as well.

The reduced miR-493 expression in primary tumours with liver metastasis, but not with lung metastasis (Supplementary Figure S4F and G) suggests that the anti-metastatic effects of miR-493/miR-493* are specific to liver metastasis. The 'seeds and soil' theory of metastasis proposes that efficient formation of metastasis depends on the interaction between metastatic cells and the targeted organs in a tumour microenvironment (Nguyen *et al*, 2009; Psaila and Lyden, 2009; Langley and Fidler, 2011). In this context, clarification of miR-493 function may aid future understanding of why colon cancer cells preferentially metastasize in the liver.

While the expression of miR-493 and miR-493* is highly correlated in primary colon tumours, expression of pre-miR-493, their precursor, is not related to either. These observations suggest that the processing of pre-miR-493 may play a regulatory role in the induction of miR-493/miR-493* during carcinogenesis. Recently, it has been shown that some of the crucial regulators against carcinogenesis, such as p53, ATM, or TGF- β , are involved in the processing of miRNA precursors (Suzuki and Miyazono, 2011; Zhang *et al*, 2011).

miR-493 expression induced cell death of the metastasized cells concomitantly with their disappearance from the liver (Figure 3). Therefore, it is likely that induction of cell death is the mechanism by which miR-493 inhibits liver metastasis. Interestingly, both miR-493 and miR-493* were capable of inhibiting phosphorylation of Akt (Figure 4B), and the inhibitory function of these miRNAs on Akt may contribute to the reduced survival of cells that were metastasized in liver. On the other hand, we found that miR-493 expression decreases invasion activity in standard Matrigel assays (Supplementary Figure S2C). Considering that HCT116 is EMT (-) cells that express high levels of E-cadherin (Park *et al*, 2008), it is not clear whether a further decrease of invasiveness of HCT116 cells is involved in the inhibition of liver metastasis in our assays.

Our data in Figure 4 firmly established IGF1R as a novel target of miR-493. IGF1R promotes the survival and metastasis of several types of cancer, including colorectal cancer (Ewing and Goff, 2010), and is regarded as a potent therapeutic target against them (Chitnis *et al*, 2008; Ewing and Goff, 2010). In fact, blockade of its ligand using neutralizing antibodies reduces liver metastasis of colorectal cancer cells (Miyamoto *et al*, 2005). In accordance, our data indicate that IGF1R enhances liver metastasis (Figure 4G), and promotes cell survival in the liver (Figure 4H). Thus, it is likely that enhanced survival of IGF1R is partly responsible for the function of miR-493 to inhibit metastasis, although the suppression of IGF1R alone cannot explain the inhibitory function of miR-493 (Supplementary Figure S3D), and there are possibly other target genes that co-operate with IGF1R. Future investigation will clarify the full picture of miR-493 targets and their functions on liver metastasis.

Given the metastasis-inhibitory function of miR-493, increasing levels of miR-493 may be effective in preventing liver metastasis, especially for patients who suffer from primary colon cancer with low levels of miR-493. Given the potential of miRNAs for therapeutic applications (Trang *et al*, 2008; Iguchi *et al*, 2010; Petrocca and Lieberman, 2011), this may be done by administering miR-493 or its agonist analogues. Alternatively, stimulation of the processing of its precursor may induce levels of endogenous miR-493. In either case,

elevation of miR-493 levels may become an effective adjuvant therapy against liver metastasis in the future.

Materials and methods

Cell lines and plasmids

All colon cancer cells and their derivatives were cultivated in Dulbecco's MEM supplemented with 10% FCS. miRNA precursor-expressing lentivirus plasmids were purchased from System Biosciences (CA, USA). In order to create a lentivirus plasmid that expresses IGF1R, an IGF1R cDNA fragment was amplified from FHC-derived cDNA and ligated into pLenti6-DEST (Invitrogen). A luciferase reporter for 3'UTR of IGF1R (psicheck-IGF1R-UTR) was created by inserting a 420-bp 3'UTR DNA fragment spanning the predicted miR-493 target site into the 3' end of Renilla luciferase of psicheck2, a dual-luciferase reporter plasmid (Promega). A luciferase reporter with the mutated 3'UTR (psicheck-IGF1R-UTR-mut) was generated by substituting five nucleotides at the miR-493 target site with *In Vitro* Mutagenesis kit (Stratagene).

Lentivirus production and infection

Lentivirus plasmids were co-transfected with pLP1, pLP2, and pLP/VSVG (Invitrogen) into 293FT cells (Invitrogen), and virus-containing supernatants were prepared according to manufacturer's instructions. For lentivirus infection, cells were incubated with virus-containing supernatants in the presence of 6 μ g/ml polybrene. For infection of the lentiviruses that express IGF1R or their control viruses, infected cells were selected in the presence of 8 μ g/ml blasticidin. For infection of GFP-expressing viruses for miRNA expression, flow cytometry analyses (FacsCalibur, Becton Dickinson) were performed to confirm that >90% of cells were infected.

Functional screening of miRNAs that inhibit liver metastasis

HCT116 cells were infected with a human miRNA precursor expression lentivirus library that expresses GFP (System Biosciences) with 6 μ g/ml polybrene. Judging from a fraction of GFP-positive cells, 80–90% of cells were infected with the virus. A pool of library-infected cells (1×10^6 cells) was suspended in medium containing 50% Matrigel (Becton Dickinson), and injected into the spleens of 8-week-old NOG (NOD/Shi-*scid* IL2r^{g^{tm1}}) mice (Central Institute for Experimental Animals, Tokyo, Japan).

Two weeks after the splenic injection, dissected livers and spleens were minced, treated with 1 μ g/ μ l DNase I (Roche Applied Science) and 1 mg/ml collagenase I (Roche Applied Science) for 30 min at 37°C, and filtered with a 100- μ m cell strainer (BD Falcon). Subsequently, the library-introduced cells were isolated through centrifugal purification in phosphate-buffered saline containing Histodenz (Sigma, MO, USA). Isolation of genomic DNA, amplification and Cy5/Cy3 labelling of DNA fragments spanning library-introduced miRNA, and analyses of Cy5/Cy3 ratio of each miRNA using the custom-made microarrays were performed as previously described (Izumiya *et al*, 2010).

Liver metastasis assays

HCT116 cells were infected with lentiviruses that express miRNA and GFP (System Biosciences) or with control lentiviruses in the presence of 6 μ g/ml polybrene. Alternatively, HCT116/GFP or DLD-1/GFP (2×10^5 cells) cells were transfected with 4 pmoles of siRNAs (Invitrogen) or 6 pmoles of miRNA mimics (pre-miR miRNA precursors; Ambion) in the presence of 20 μ l Hiperfect (Qiagen) for 2 days. Subsequently, the GFP-positive cells were mixed with HCT116/RFP or DLD-1/RFP at a 1:1 ratio, suspended in normal growth medium containing 50% Matrigel, and injected into spleen of NOG mice ($2-4 \times 10^5$ cells). A fraction of the cell mixture before the injection was used for flow cytometry analyses to accurately measure original ratios of GFP/RFP-positive cells.

In all, 1–14 days after splenic injection, the inhibitory effects of siRNA or miRNA on liver metastasis were evaluated by GFP/RFP imaging (OV110; Olympus), or by measuring the ratios of GFP/RFP-positive cells by flow cytometry after recovering metastasized cells from livers as described above. The inhibitory effect of each oligonucleotide was calculated by comparing the GFP/RFP ratios before and after liver metastasis.

Cell death assays of metastasized cells

HCT116/RFP cells were transfected with miRNA mimics as described above, and 4×10^5 of the transfected cells were injected into the spleens of NOG mice. Three days after the splenic injection, Alexa 488-labelled Annexin V (Molecular Probe, OR, USA) was injected into the tail vein for 1 h, and the number of Alexa 488-positive HCT116/RFP cells in the dissected liver was counted by fluorescence microscopy.

Western blot analyses

Cells were lysed in RIPA buffer and used for western blot analyses as previously described (Okamoto *et al*, 2005), with anti-IGF1R (Cell Signaling), anti-Actin (Sigma), anti-Akt (Cell Signaling), or anti-phospho-Akt (PS473) (Cell Signaling).

RNA preparation and RT-qPCR analysis

RNA was isolated from cells with miRNeasy Mini kit (Qiagen), and levels of miRNAs or genes were measured by performing Taqman microRNA assays or Taqman gene expression assays (Applied Biosystems) according to manufacturer's instructions. RNU48 or Actin expression was used to calculate delta Ct values for miRNA or genes, respectively.

Luciferase reporter assays

A dual-luciferase reporter construct with or without 3'UTR of IGF1R was transfected into HCT116/GFP cells in the presence of a miR-493 mimic or its control, and Firefly and Renilla luciferase activities were measured by the Dual-Luciferase Reporter System (Promega) 2 days after transfection.

Matrigel invasion assays

Ten thousand transfected HCT116 cells were serum starved with medium with 0.1% serum overnight, and seeded onto 24-well Matrigel-coated inserts (8 μ m pore; BD Falcon). After 24 h, cells attached to the lower surfaces of the insert filter were counted after staining with the Diff-Quick staining kit (Sysmex, Tokyo).

Immunohistochemical analysis

Metastasized mouse liver was fixed in formalin, embedded in paraffin, sectioned, and stained with HE or with standard immunohistochemistry methods. For immunostaining with E-cadherin, deparaffinized sections were incubated with an anti-E-cadherin antibody (Santa-Cruz), and biotinylated anti-mouse secondary antibody followed by ABC reagent and DAB (Vector Laboratories). The slides were counterstained with haematoxylin. For IGF1R immunostaining of human primary cancer, freshly frozen samples of human primary colon tumours were sectioned, fixed in acetone, and immunostained with anti-IGF1R antibody (Cell Signaling). Staining with the secondary antibody and the detection steps were performed as described above. The extent of the staining was visually evaluated on a scale of 0 (no staining) to 3 (strong staining). Approximately 800 cells were evaluated for each sample by two observers, and the mean value for each staining was calculated.

References

- Bartel DP (2009) MicroRNAs: target recognition and regulatory functions. *Cell* **136**: 215–233
- Bouvet M, Tsuji K, Yang M, Jiang P, Moossa AR, Hoffman RM (2006) *In vivo* color-coded imaging of the interaction of colon cancer cells and splenocytes in the formation of liver metastases. *Cancer Res* **66**: 11293–11297
- Chaffer CL, Weinberg RA (2011) A perspective on cancer cell metastasis. *Science* **331**: 1559–1564
- Chambers AF, Groom AC, MacDonald IC (2002) Dissemination and growth of cancer cells in metastatic sites. *Nat Rev Cancer* **2**: 563–572
- Chitnis MM, Yuen JS, Protheroe AS, Pollak M, Macaulay VM (2008) The type 1 insulin-like growth factor receptor pathway. *Clin Cancer Res* **14**: 6364–6370

Clinical specimens

Tumour and non-tumour tissues were resected from patients with informed consent at the Teikyo University Hospital, and all procedures were performed under the protocol approved by the Ethics Committee of Teikyo University Hospital. Each case without metastasis at the time of surgery was subjected to a 2-year follow-up for classification of the metastatic status. RNAs were purified from dissected samples, and a part of each tumour was freshly frozen for immunostaining.

Microarray analyses

Total RNA was extracted from the transfected HCT116 cells using miRNeasy mini kit (Qiagen). Purified RNA was labelled with Cy3 dye, and hybridized to Agilent Whole Human Genome 4 \times 44K Oligo Microarrays according to manufacturer's instructions (Agilent Technologies). Microarray data are analysed using Genespring software (Agilent Technologies), and accessible through the Gene Expression Omnibus (GEO) database (GEO Series accession number GSE31751).

Statistical analysis

Statistical analyses were performed by JMP (6.0) software (SAS Institute, NC, USA). Data included in Figure 5A–D and Supplementary Figure S4 were subjected to one-way ANOVA. The other data were analysed by the two-tailed Student's *t*-test. All data are presented as the mean \pm s.d.

Supplementary data

Supplementary data are available at *The EMBO Journal* Online (<http://www.embojournal.org>).

Acknowledgements

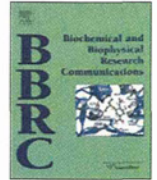
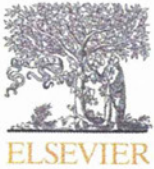
We thank Yoshinori Ikarashi for fluorescent imaging; Shigeki Sekine for immunohistochemical analyses; Masako Ochiai for statistical analyses; and Ibuki Kobayashi, Kazuhiro Kanemoto, and Yuki Tabe for technical assistance. NOG mice were provided by the Central Institute for Experimental Animal (Tokyo, Japan). This research was supported by a Grant-in-Aid for the Third-Term Comprehensive 10-Year Strategy for Cancer Control from the Ministry of Health, Labor and Welfare; the Program for Promotion of Fundamental Studies in Health Sciences of the National Institute of Biomedical Innovation (NiBio). TI is a recipient of a Research Resident Fellowship from the Foundation for Promotion of Cancer Research (FPCR, Japan). None of the authors have a financial interest related to this work.

Author contributions: KO designed and performed experiments, analysed data and wrote the manuscript. YM performed experiments and analysed data. MI and NT designed and performed experiments. TI, HO, AS, and HS performed experiments. HN designed experiments and wrote the manuscript.

Conflict of interest

The authors declare that they have no conflict of interest.

- Hamada K, Monnai M, Kawai K, Nishime C, Kito C, Miyazaki N, Ohnishi Y, Nakamura M, Suemizu H (2008) Liver metastasis models of colon cancer for evaluation of drug efficacy using NOD/Shi-scid IL2Rgammamnull (NOG) mice. *Int J Oncol* **32**: 153–159
- Hermeking H (2007) p53 enters the microRNA world. *Cancer Cell* **12**: 414–418
- Hess KR, Varadhachary GR, Taylor SH, Wei W, Raber MN, Lenzi R, Abbruzzese JL (2006) Metastatic patterns in adenocarcinoma. *Cancer* **106**: 1624–1633
- Huang Q, Gumireddy K, Schrier M, le Sage C, Nagel R, Nair S, Egan DA, Li A, Huang G, Klein-Szanto AJ, Gimotty PA, Katsaros D, Coukos G, Zhang L, Pure E, Agami R (2008) The microRNAs miR-373 and miR-520c promote tumour invasion and metastasis. *Nat Cell Biol* **10**: 202–210
- Iguchi H, Kosaka N, Ochiya T (2010) Versatile applications of microRNA in anti-cancer drug discovery: from therapeutics to biomarkers. *Curr Drug Discov Technol* **7**: 95–105
- Iorio MV, Croce CM (2009) MicroRNAs in cancer: small molecules with a huge impact. *J Clin Oncol* **27**: 5848–5856
- Izumiya M, Okamoto K, Tsuchiya N, Nakagama H (2010) Functional screening using a microRNA virus library and microarrays: a new high-throughput assay to identify tumor-suppressive microRNAs. *Carcinogenesis* **31**: 1354–1359
- Izumiya M, Tsuchiya N, Okamoto K, Nakagama H (2011) Systematic exploration of cancer-associated microRNAs through functional screening assays. *Cancer Sci* **102**: 1615–1621
- Langley RR, Fidler IJ (2011) The seed and soil hypothesis revisited—the role of tumor-stroma interactions in metastasis to different organs. *Int J Cancer* **128**: 2527–2535
- le Sage C, Nagel R, Egan DA, Schrier M, Mesman E, Mangiola A, Anile C, Maira G, Mercatelli N, Ciafre SA, Farace MG, Agami R (2007) Regulation of the p27 (Kip1) tumor suppressor by miR-221 and miR-222 promotes cancer cell proliferation. *EMBO J* **26**: 3699–3708
- Lotterman CD, Kent OA, Mendell JT (2008) Functional integration of microRNAs into oncogenic and tumor suppressor pathways. *Cell Cycle* **7**: 2493–2499
- Miyamoto S, Nakamura M, Shitara K, Nakamura K, Ohki Y, Ishii G, Goya M, Kodama K, Sangai T, Maeda H, Shi-Chuang Z, Chiba T, Ochiai A (2005) Blockade of paracrine supply of insulin-like growth factors using neutralizing antibodies suppresses the liver metastasis of human colorectal cancers. *Clin Cancer Res* **11**: 3494–3502
- Nguyen DX, Bos PD, Massague J (2009) Metastasis: from dissemination to organ-specific colonization. *Nat Rev Cancer* **9**: 274–284
- Nicoloso MS, Spizzo R, Shimizu M, Rossi S, Calin GA (2009) MicroRNAs—the micro steering wheel of tumour metastases. *Nat Rev Cancer* **9**: 293–302
- Okamoto K, Kashima K, Pereg Y, Ishida M, Yamazaki S, Nota A, Teunisse A, Migliorini D, Kitabayashi I, Marine JC, Prives C, Shiloh Y, Jochemsen AG, Taya Y (2005) DNA damage-induced phosphorylation of MdmX at serine 367 activates p53 by targeting MdmX for Mdm2-dependent degradation. *Mol Cell Biol* **25**: 9608–9620
- Park SM, Gaur AB, Lengyel E, Peter ME (2008) The miR-200 family determines the epithelial phenotype of cancer cells by targeting the E-cadherin repressors ZEB1 and ZEB2. *Genes Dev* **22**: 894–907
- Petrocca F, Lieberman J (2011) Promise and challenge of RNA interference-based therapy for cancer. *J Clin Oncol* **29**: 747–754
- Psaila B, Lyden D (2009) The metastatic niche: adapting the foreign soil. *Nat Rev Cancer* **9**: 285–293
- Schlabach MR, Luo J, Solimini NL, Hu G, Xu Q, Li MZ, Zhao Z, Smogorzewska A, Sowa ME, Ang XL, Westbrook TF, Liang AC, Chang K, Hackett JA, Harper JW, Hannon GJ, Elledge SJ (2008) Cancer proliferation gene discovery through functional genomics. *Science* **319**: 620–624
- Shibue T, Weinberg RA (2011) Metastatic colonization: settlement, adaptation and propagation of tumor cells in a foreign tissue environment. *Semin Cancer Biol* **21**: 99–106
- Suzuki HI, Miyazono K (2011) Emerging complexity of microRNA generation cascades. *J Biochem* **149**: 15–25
- Tazawa H, Tsuchiya N, Izumiya M, Nakagama H (2007) Tumor-suppressive miR-34a induces senescence-like growth arrest through modulation of the E2F pathway in human colon cancer cells. *Proc Natl Acad Sci USA* **104**: 15472–15477
- Trang P, Weidhaas JB, Slack FJ (2008) MicroRNAs as potential cancer therapeutics. *Oncogene* **27** (Suppl 2): S52–S57
- Tsuchiya N, Izumiya M, Ogata-Kawata H, Okamoto K, Fujiwara Y, Nakai M, Okabe A, Schetter AJ, Bowman ED, Midorikawa Y, Sugiyama Y, Aburatani H, Harris CC, Nakagama H (2011) Tumor suppressor miR-22 determines p53-dependent cellular fate through post-transcriptional regulation of p21. *Cancer Res* **71**: 4628–4639
- Ventura A, Jacks T (2009) MicroRNAs and cancer: short RNAs go a long way. *Cell* **136**: 586–591
- Voorhoeve PM, Agami R (2007) Classifying microRNAs in cancer: the good, the bad and the ugly. *Biochim Biophys Acta* **1775**: 274–282
- Voorhoeve PM, le Sage C, Schrier M, Gillis AJ, Stoop H, Nagel R, Liu YP, van Duijse J, Drost J, Griekspoor A, Zlotorynski E, Yabuta N, De Vita G, Nojima H, Looijenga LH, Agami R (2006) A genetic screen implicates miRNA-372 and miRNA-373 as oncogenes in testicular germ cell tumors. *Cell* **124**: 1169–1181
- Vousden KH, Prives C (2009) Blinded by the light: the growing complexity of p53. *Cell* **137**: 413–431
- Wang J, Yang M, Hoffman RM (2004) Visualizing portal vein metastatic trafficking to the liver with green fluorescent protein-expressing tumor cells. *Anticancer Res* **24**: 3699–3702
- Winter J, Jung S, Keller S, Gregory RI, Diederichs S (2009) Many roads to maturity: microRNA biogenesis pathways and their regulation. *Nat Cell Biol* **11**: 228–234
- Wu WK, Law PT, Lee CW, Cho CH, Fan D, Wu K, Yu J, Sung JJ (2011) MicroRNA in colorectal cancer: from benchtop to bedside. *Carcinogenesis* **32**: 247–253
- Zhang X, Wan G, Berger FG, He X, Lu X (2011) The ATM kinase induces microRNA biogenesis in the DNA damage response. *Mol Cell* **41**: 371–383



Differential expression of *nanog1* and *nanogp8* in colon cancer cells

Tatsuya Ishiguro^{a,1}, Ai Sato^{a,1}, Hirokazu Ohata^a, Hiroaki Sakai^a, Hitoshi Nakagama^{b,*}, Koji Okamoto^{a,*}

^aDivision of Cancer Differentiation, National Cancer Center Research Institute, 5-1-1 Tsukiji, Chuo-ku, Tokyo 104-0045, Japan

^bDivision of Cancer Development System, National Cancer Center Research Institute, 5-1-1 Tsukiji, Chuo-ku, Tokyo 104-0045, Japan

ARTICLE INFO

Article history:

Received 25 October 2011

Available online 31 October 2011

Keywords:

Cancer
Stem cells
Nanog

ABSTRACT

Nanog, a homeodomain transcription factor, is an essential regulator for promotion of self-renewal of embryonic stem cells and inhibition of their differentiation. It has been demonstrated that *nanog1* as well as *nanogp8*, a retrogene of *nanog1*, is preferentially expressed in advanced stages of several types of cancer, suggesting their involvement during cancer progression. Here, we investigated the expression of Nanog in well-characterized colon cancer cell lines. Expression of Nanog was detectable in 5 (HCT116, HT29, RKO, SW48, SW620) out of seven cell lines examined. RNA expression analyses of *nanog1* and *nanogp8* indicated that, while *nanog1* was a major form in SW620 as well as in teratoma cells Tera-2, *nanogp8* was preferentially expressed in HT29 and HCT116. In accordance with this, shRNA-mediated knockdown of *nanog1* caused the reduction of Nanog in SW620 but not in HT29. Inhibition of Nanog in SW620 cells negatively affected cell proliferation and tumor formation in mouse xenograft. Biochemical subcellular fractionation and immunostaining analyses revealed predominant localization of Nanog in cytoplasm in SW620 and HT29, while it was mainly localized in nucleus in Tera-2. Our data indicate that *nanog1* and *nanogp8* are differentially expressed in colon cancer cells, and suggest that their expression contributes to proliferation of colon cancer cells.

© 2012 Published by Elsevier Inc.

1. Introduction

It has been well documented that a set of transcription factors, Oct-3/4, Nanog, and Sox-2, controls self-renewal and pluripotency of embryonic stem (ES) cells [1]. Accumulating reports indicate that these transcription factors, in combination with a set of regulatory microRNAs and transcriptional co-regulators that modify chromatin structure, form a key regulatory network controlling the identity and differentiation of ES cells [2–4].

Recent progress on cancer research revealed that, among the ES-specific transcription factors, Oct-3/4 and Nanog are expressed in a variety of human cancers [5–8]. Especially, expression of Nanog is associated with advanced stage and poor prognosis in some types of cancer [6,9–11].

Nanog is a homeodomain transcription factor that plays a crucial role in maintaining integrity of undifferentiated ES cells, and regulated by a variety of extrinsic and intrinsic signals [12]. Whereas external signal factors including HIF [13], Hedgehog (HH) [14,15], LIF [16], and TGF- β /activin/nodal [17,18] as well as the intrinsic transcription regulators such as Oct-3/4 and Sox-2 [19,20], SMAD [18], Klf4 [21,22], GLI1 [14,15], SATB [23], mSi-

n3A-HDAC [24], β -catenin [25], and Sall4 [26] function to transcriptionally up-regulate Nanog expression, the induction of p53 [27,28] or epigenetic modification of its promoter [29,30] inhibits its expression. Nanog expression is also regulated by ES-specific microRNAs [31,32]. Activated Nanog, in a complex of associated transcription co-factors [33–35], in turn regulates gene transcription of its targets to promote self-renewal of embryonic stem cells and affects differentiation processes [2,34,36]. Presumably through the regulation of the expression of the target genes, Nanog functions to transit to a ground state for pluripotency of ES cells [37], and blocks their differentiation [38].

In addition to *nanog1*, an authentic gene that encodes Nanog, there are 10 pseudogenes for Nanog in the human genome [39,40]. Among them, *nanogp8* is the most recent pseudogene generated during evolution [39], and is regarded as a retrogene because it retains the capacity to code for a 305 amino acid polypeptide that is structurally very similar to the *nanog1* gene product [40], and is expressed in human cells [41]. In fact, ectopic expression of *nanogp8* generates the functional protein [41,42]. Because of high degree of homology between these genes, the protein products of *nanog1* and *nanogp8* are basically indistinguishable on western blot analyses or immunostaining [41,43]. Therefore, protein products of these genes are collectively referred to as Nanog [42,43].

Examination of Nanog expression in clinical studies revealed that Nanog is overexpressed in a variety of cancer [5–11,44,45].

* Corresponding authors. Fax: +81 3 3542 2980 (K. Okamoto).

E-mail addresses: hnakagam@ncc.go.jp (H. Nakagama), kojokamo@ncc.go.jp (K. Okamoto).

¹ These authors equally contributed to this work.

Indeed, expression of *nanog1* gene was demonstrated at least in some of cancer cell lines [46], and ectopic expression of *nanog1* contributes to stem cell-like properties to cells [5] and promotes cell proliferation [47]. Of note, *nanogp8* gene is rather a major form expressed in many types of cancer [15,41,42], promotes stem cell-like characteristics [15,43], and facilitates progression of cancer [15,41,42]. Thus, it is likely that both *nanog1* and *nanogp8* contribute to cancer development mediated by Nanog.

In human colon cancer, high levels of Nanog expression are associated with advanced stages of cancer and poor prognosis [10]. It is likely that expression of Nanog in colon cancer is functionally important because *nanog1* over-expression in colon cancer cells promotes its proliferation [10]. However, it remains unclear whether *nanog1* or *nanogp8* is a major form that is expressed in colon cancer cells, and the expression and subcellular localization of Nanog in those cells have not been well documented. These issues should be clarified to understand the molecular mechanisms of Nanog in colon cancer development.

In this paper, we investigated expression of Nanog in a set of well-characterized human colon cancer cells. Our data indicate that, while both *nanog1* and *nanogp8* are expressed in most colon cancer cells, they are expressed at varied ratios dependent on cell lines. Examination of subcellular localization indicates Nanog is mainly localized in cytoplasm in at least two colon cancer cells. In addition, Nanog inhibition by shRNAs in colon cancer cells caused growth inhibition in *in vitro* culture and in mouse xenograft, indicating the positive role of Nanog in proliferation of colon cancer cells.

2. Materials and methods

2.1. Cell culture

All colon cancer cells and Tera-2 were cultivated in Dulbecco's modified Eagle medium (Invitrogen) supplemented with 10% fetal bovine serum (Invitrogen). FHC cells were cultivated in a 1:1 mixture of Ham F-12 medium and Dulbecco's modified Eagle medium (Invitrogen) supplemented with 25 mM Hepes (Invitrogen), 10 ng/ml cholera toxin (Calbiochem), 5 µg/ml insulin (Sigma), 5 µg/ml transferrin (Sigma), 100 ng/ml hydrocortisone (Sigma), and 10% fetal bovine serum (Invitrogen).

2.2. Western blot analyses

Cells were lysed in lysis buffer (50 mM Tris at pH 8.0, 150 mM NaCl, 1% Nonidet P-40, 0.5% sodium deoxycholate, 0.1% SDS and 1 mM EDTA) supplemented with protease inhibitors, and used for Western blot analyses as previously described [48], with anti-Nanog (ReproCELL, Tokyo), anti-Oct-3/4 (C-10, Santa Cruz Biotechnology), anti-Sox-2 (H-65, Santa Cruz Biotechnology), anti-Actin (Sigma, A5316), anti-Topol (C-21, Santa Cruz Biotechnology), or anti-beta-Tubulin (D-10, Santa Cruz Biotechnology).

2.3. Lentivirus preparation and Infection

Lentiviral plasmid vectors expressing *Nanog1* shRNAs (#1, #2) or control shRNAs (#1, #2) were purchased from Sigma (the Mission shRNA clones). Note that *nanog1* shRNA (#2) corresponds to the older version of *nanog1* sequence (NM_024865.1) but not to the current version (NM_024865.2). Lentiviruses that express GFP or RFP (pCDH-CMV-MCS-EF1) were purchased from System Biosciences (CA, USA). The lentiviral plasmids were co-transfected with pLP1, pLP2 and pLP/VSVG (Invitrogen) into 293FT cells (Invitrogen), and virus-containing supernatants were prepared according to the manufacturer's instructions. For infection of the

lentiviruses, SW620 cells were incubated with virus-containing supernatants in the presence of 6 µg/ml polybrene. Cells infected with the shRNA-expressing viruses or the control viruses were selected in the presence of 1 µg/ml puromycin. For cells infected with GFP or RFP-expressing viruses, flow cytometry analyses (FacsCalibur, Becton Dickinson) were performed to confirm that >90% of cells were infected.

2.4. RT-PCR analyses

Complementary DNA (cDNA) was synthesized from total RNA using a PrimeScript 1st strand cDNA Synthesis Kit (Takara). For amplification of *nanog* cDNA, the PCR reaction with the cDNA was performed with ExTaq (Takara) for 35 cycles with the following conditions: 94 °C (1 min), 68 °C (1 min), 72 °C (2 min). For amplification of *gapdh* cDNA, the PCR reaction was performed for 30 cycles with the following conditions: 94 °C (1 min), 55 °C (1 min), 72 °C (2 min). The following primer sets were used for PCR reactions: *Nanog* forward primer (5'-AACATGAGTGTGGATC-CAG-3'), *Nanog* reverse primer (5'-TCACTCATCTTCACAGTCTT-CAGTTG-3'), *GAPDH* forward primer (5'-ACCACAGTCCAGTCCA TCAC-3'), *GAPDH* reverse primer (5'-TCCACCACCCTGTTGCTGTA-3').

2.5. Subcellular fractionation

Cells were rinsed in 1× phosphate-buffered saline (PBS), and cytoplasmic and nuclear fractions were prepared using the NEPER Nuclear and Cytoplasmic Extraction Reagents according to the manufacturer's instructions (Thermo Scientific). The prepared lysates were used for western blot analyses.

2.6. Immunostaining

Cells were fixed in 4% paraformaldehyde in PBS for 15 min, washed with 1× PBS, permeabilized in PBS/0.1% Triton X-100 for 5 min at 4 °C, and blocked with PBS containing 3% bovine serum albumin (BSA). The fixed cells were then used for immunostaining with anti-Nanog (ReproCELL) and DAPI.

2.7. GFP/RFP competition assays

The GFP-expressing SW620 cells were infected with the lentiviruses that express *Nanog* shRNA or the control viruses, selected in the presence of 1 µg/ml puromycin, and mixed with RFP-expressing SW620 at a 1:1 ratio, and used for an *in vitro* culture. For mouse xenograft experiments, the infected cells (1×10^6 cells) were suspended in medium containing 50% Matrigel (Becton Dickinson), and subjected for subcutaneous injection into NOG (NOD/Shi-*scid* *IL-2rg^{null}*) mice. The inhibitory effects of *Nanog* shRNAs were evaluated by measuring the number of GFP/RFP-positive cells by flow cytometry, and calculating the reduction of GFP/RFP ratios after these experimental procedures.

3. Results and discussion

3.1. *Nanog* is expressed in a majority of colon cancer cell lines

In order to examine whether ES-specific transcription factors, *Nanog*, *Oct3/4*, and *Sox2* are expressed in colon cancer cells, we performed western blot analyses of seven colon cancer cells (DLD-1, HCT116, HT29, RKO, SW48, SW480, SW620) as well as normal colon epithelial cells (FHC) and teratoma cells (Tera-2). We observed detectable levels of *Nanog* and *Sox-2* expression in most cell lines, whereas *Oct3/4* was not detected in any colon cancer cells